in culture medium (84.9±5.2 in a.u., n = 6, *P<0.01* versus control), indicating that LPS treatment induced secretion of MMP-9 from cells to culture medium. In the case of cells pretreated with donepezil (DPZ/LPS), intracellular MMP-9 was undetectable levels like that in donepezil-pretreated culture medium (cell, 29.1±1.9 in a.u., n = 6, *P<0.01* versus control, *P<0.01* versus LPS and medium, 34.4±10.5 in a.u., n = 6, *P<0.05* versus control, *P<0.01* versus LPS). It was also observed that donepezil pretreatment reduced MMP-9 content within cells not treated with LPS (data not shown). These results indicate that donepezil suppresses the de novo synthesis of MMP-9 during the pretreatment period, resulted in the lower content of MMP-9 in the culture medium even after the LPS treatment. Gelatin zymography was carried out to analyze the enzymatic activity of MMP-9 secreted to culture medium (Figure 3b). Although pro- and active-forms of MMP-9 could not be clearly distinguished, MMP-9 retained its proteinase activity even after being secreted to culture medium. The signal intensity of MMP-9 was significantly high in LPS-treated cells (LPS, 119.33±10.73% versus control, n = 6, *P<0.01*) and low in donepezil-pretreated and LPS-treated cells (DPZ/LPS, 83.52±2.59% versus control, n = 6, *P<0.01*), compared to control (control, 100.00±14.3%, n = 6).

The effect of donepezil on the macrophage MMP-9 was further examined by immunocytochemistry (Figure 4). Isolated and cultured macrophages were observed to attach well to a substratum and form widespreading pseudopodia. Compared to the control that showed a high proportion of cells with spindle shapes (Figure 4a), LPS-treated cells displayed a relatively round shape and a numerous intracellular vacuoles (Figure 4c). Such morphological alterations induced by LPS treatment were also observed in donepezil-pretreated cells (Figure 4e), indicating that the donepezil pretreatment had no effect on the macrophage reactivity to LPS treatment. Immunofluorescence microscopy with anti MMP-9 antibody showed that MMP-9 was distributed around cytoplasm in control and LPS-treated cells (Figures 4b and d), whereas donepezil decreased the immunoreactivities of MMP-9 within cytoplasm (Figure 4f). These results indicate that the donepezil pretreatment decreased MMP-9 content within the cell, which coincided with the results obtained immunoblot analysis shown in Figure 3a.

Effect of donepezil on risk of cardiac rupture after myocardial infarction

A total of 330 mice was operated (310 mice were subjected to coronary artery ligation, whereas 20 mice underwent sham operation) and 60 mice (18.2%) died within 24 hrs due to surgical reasons. No deaths were observed in the sham-operated mice. Ten mice (3.7%) that died during the follow up period (4 days postinfarction) without diagnosis of cardiac rupture and 37 mice (13.7%) that had obviously small left ventricular infarction were excluded from the study. Consequently, 223 mice were allocated into examining an incidence of rupture, heart rate (HR) and systolic blood pressure (SBP) measurement, histology, immunohistochemistry, and tissue collection for RT-PCR, Western blot analysis and gelatin zymography. Surviving mice with myocardial infarction (MI) were divided into 2 groups; untreated and donepezil-treated (DPZ) groups.

HR and SBP were measured noninvasively using a computer-automated tail-cuff system in sham-operated and infarcted mice at day 3 after surgery. As shown in Table 1, there was no significant difference in HR among all groups of mice (sham, 493±70 bpm, n = 6; untreated, 548±53 bpm, n = 9 and DPZ, 528±43 bpm, n = 9, N.S.). On the other hand, SBP was decreased significantly in infarcted groups (untreated, 81.6±7.4 mmHg, n = 9, *P<0.01* and DPZ, 78.3±7.9 mmHg, n = 9, *P<0.01*) compared with the sham group (98.9±5.0 mmHg, n = 6), indicating a progression of cardiac dysfunction after MI. However, values of the decreased SBP in the infarcted groups were comparable. In another set of experiments showed that no significant differences in HR and SBP were observed in normal mice treated with donepezil (DPZ, 5.0 mg/kg/day) for 3 days (HR, 504±36 bpm, n = 6 and SBP, 103.7±9.8 mmHg, n = 6). These results indicate that the donepezil administration at the dosage of 5.0 mg/kg/day did not affect HR and SBP in normal and infarcted mice. When mice were sacrificed at 3 days after MI, all excised hearts were weighed. The ratio of heart weight to body weight (HW/BW) was significantly increased in infarcted groups (untreated, 5.85±0.66 mg/g, n = 11, *P<0.01* and DPZ, 5.60±0.39 mg/g, n = 11, *P<0.01*) compared with the sham group (4.31±0.25 mg/g, n = 7). However, no significant difference was found in HW/BW among infarcted groups, suggesting that donepezil has no effect on the postinfarct cardiac enlargement during the acute phase of MI (Table 1).

Histological analysis was performed on HE stained heart sections at 3 days after MI (Table 2). Although wall thickness of left ventricle and septum were not significantly different between untreated and donepezil-treated groups, the ratio of these in the donepezil-treated group was significantly greater than that in the untreated group (untreated, 0.51±0.07, n = 5 and DPZ, 0.69±0.20, n = 5, *P<0.05*). On the contrary, right ventricular wall thickness in the donepezil-treated group was significantly thinner than that of the untreated group (untreated, 56.1±8.91 μm, n = 5 and DPZ, 43.9±7.31 μm, n = 5, *P<0.05*). Infarct size was comparable between two groups. In the heart sections at 3 days after MI, it was observed that cardiac myocytes at mid-infarct area became necrotic and a large number of inflammatory cells infiltrated into infarct border zone. Under high power field magnification, nuclear density at the border zone of the infarct was counted and was significantly low in the donepezil-treated group compared to the untreated group (untreated, $4.42\pm0.36\times10^3/mm^2$, n = 5 and DPZ, $3.50\pm0.29\times10^3/mm^2$, n = 5, *P<0.01*).

Within 2 days after surgery, no mice were dead in all groups. Thereafter, infarcted mice began to die due to cardiac rupture at day 3 and the numbers of those mice were further increased at day 4 after MI. As described in Methods, all dead mice were immediately autopsied to determine the cause of death, and cardiac rupture was confirmed based on a diagnosis of the presence of a large amount of blood clot within the chest cavity (Figure 5a) or a wall perforation at a left ventricular infarct area (Figures 5b and c). The wall perforation tended to occur more frequently in a central region of an infarcted left ventricle or a border zone between infarcted and non-infarcted myocardium, where wall strength became relatively weak (Figure 5d). At both 3 and 4 days after MI, a greater number of animals died with rupture in the untreated group than in the donepezil-treated group, and the rupture rate of the untreated group was reached to 30.6%, whereas the donepezil-treated group showed a lower incidence of rupture (8.7%). Statistical analysis showed that, despite the comparable values of HR and SBP at day 3 after MI among infarcted groups, donepezil administration to infarcted mice significantly decreased the incidence of rupture during the acute phase of MI (*P<0.01*, Table 3).

Effect of donepezil on MMP-9 in left ventricular infarct area

As shown in Figure 6, immunofluorescence microscopy revealed that MMP-9 signals were localized at a region of an infarct left

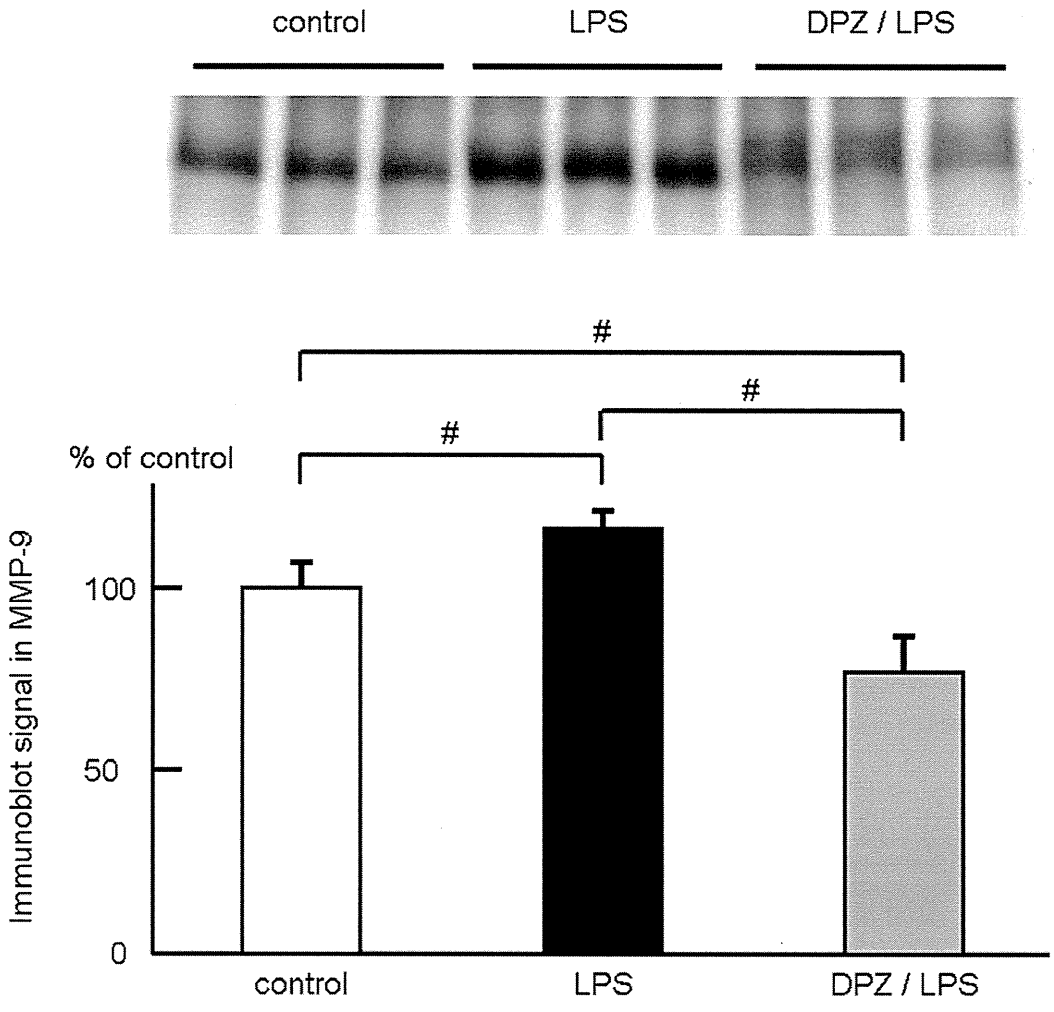

Figure 1. Effect of donepezil on MMP-9 in macrophages. MMP-9 in culture medium was evaluated by Western blot analysis before and after LPS (10 ng/ml) treatment with or without donepezil pretreatment (100 μM). Compared to control (control), LPS treatment significantly increased MMP-9 in culture medium (LPS), whereas donepezil pretreatment significantly decreased MMP-9 even in the presence of LPS (DPZ/LPS). #, $P<0.01$.
doi:10.1371/journal.pone.0020629.g001

ventricle or a border zone between infarcted and non-infarcted myocardium where a large number of nuclei were observed, suggesting that MMP-9 was produced by inflammatory cells including macrophages which infiltrated into infarct area after MI. Therefore, the effect of donepezil on the MMP-9 expression in tissues of left ventricular infarct area was examined at 3 days after MI. RT-PCR analysis showed that MMP-9 mRNA level was significantly increased (untreated, 532.60±119.24%, n = 11, $P<0.01$) compared with sham group (100.00±30.00%, n = 6), and that the increase of MMP-9 mRNA level was significantly attenuated in the donepezil-treated group (DPZ, 306.00±86.52%, n = 11, $P<0.01$) compared with the untreated group (Figure 7a). At the same time point, Western blot analysis showed that MMP-9 protein level was significantly increased in infarcted groups (untreated, 562.68±23.11%, n = 5, $P<0.01$ and DPZ, 525.75± 16.31%, n = 5, $P<0.01$) compared with sham group (100.00± 23.11%, n = 3), and was slightly but significantly decreased in the donepezil-treated group compared with the untreated group ($P<0.05$, Figure 7b). Enzymatic activity of MMP-9 in the left ventricular infarct area was evaluated by gelatin zymography at 3 days after MI (Figures 7c and d). Compared to the untreated group (untreated), signal intensity in both pro- and active-forms of MMP-9 in the donepezil-treated group (DPZ) were significantly reduced (pro MMP-9; untreated, 85.4±7.3 in a.u., n = 7 and DPZ, 74.5±6.9 in a.u., n = 7, $P<0.01$, active MMP-9; untreated, 27.7±4.5 in a.u., n = 7 and DPZ, 16.7±1.9 in a.u., n = 7, $P<0.01$, Figure 7c). Furthermore, relative enzymatic activity of MMP-9 was expressed as the ratio of active-form to total (pro- + active-form) MMP-9 signal intensity, and was significantly decreased in the donepezil-treated group compared to the untreated group (untreated, 0.24±0.02, n = 7 and DPZ, 0.18±0.01, n = 7, $P<0.01$, Figure 7d).

Discussion

Since we reported that the chronic vagal stimulation markedly improved the cardiac function and decreased mortality in a post-ischemic rat model of heart failure [3], we have focusing on elucidating the cellular and molecular mechanisms behind the ACh-induced cardioprotection. As results, vagal stimulation and

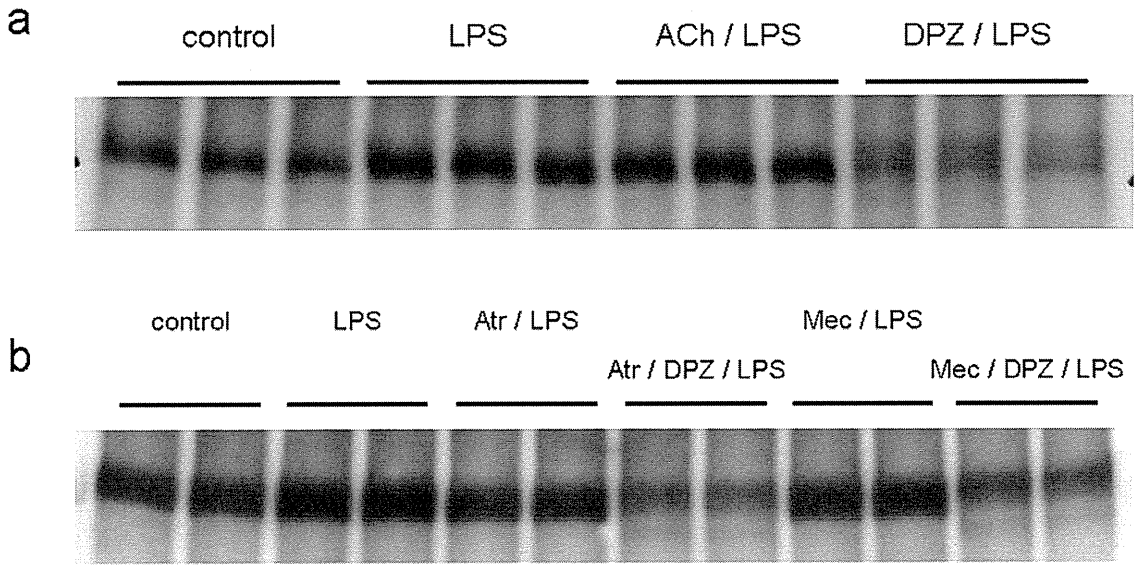

Figure 2. The involvement of ACh in the inhibitory effect of donepezil on macrophage MMP-9. (a) LPS treatment increased MMP-9 (LPS) in culture medium, which was inhibited by donepezil pretreatment (DPZ/LPS). However, ACh could not reproduce the inhibitory effect of donepezil (ACh/LPS). (b) Donepezil inhibited the LPS-induced MMP-9 even in the presence of a muscarinic ACh receptor blocker, atropine (Atr/DPZ/LPS), or a nicotinic ACh receptor blocker, mecamylamine (Mec/DPZ/LPS). Both blockers showed no effect on LPS-induced MMP-9 independently (Atr/LPS and Mec/LPS).
doi:10.1371/journal.pone.0020629.g002

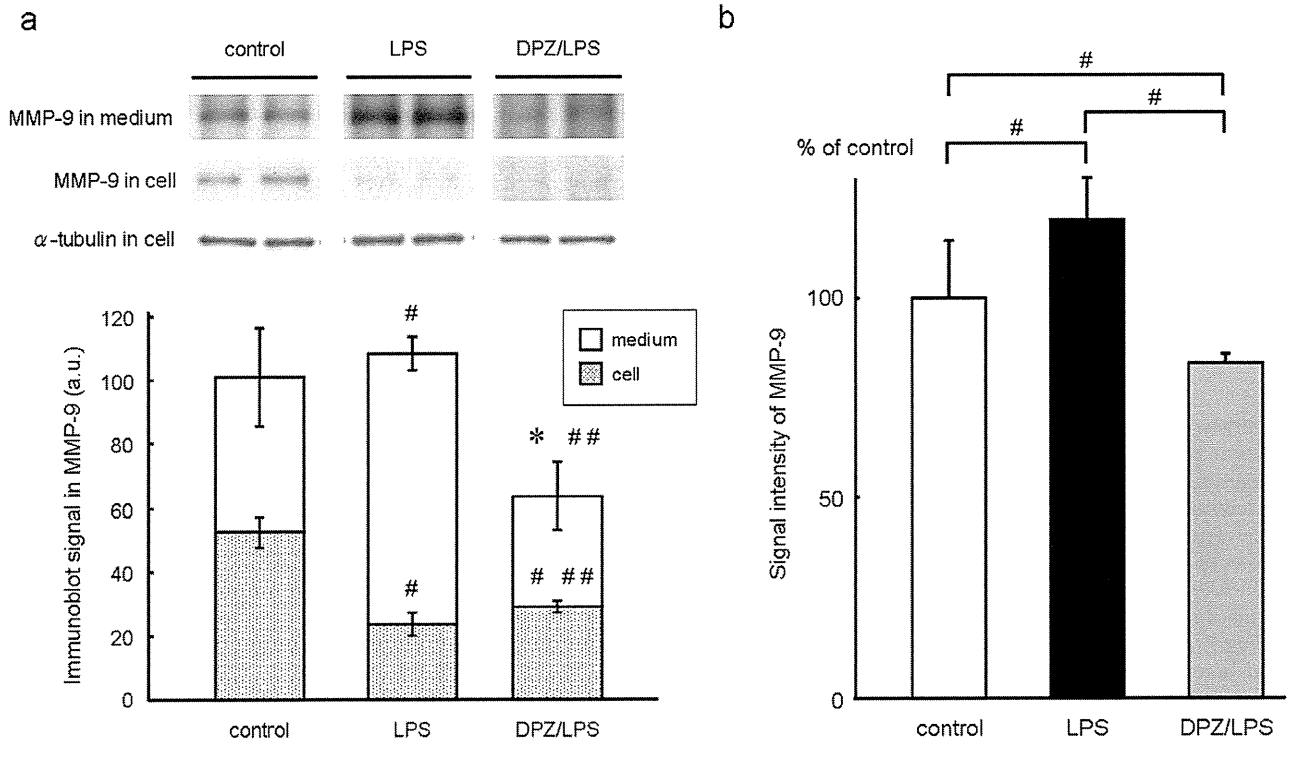

Figure 3. Western blot and zymographic analysis on macrophage MMP-9. (a) Western blot analysis of MMP-9 content in culture media and macrophage cells before and after LPS treatment with or without donepezil pretreatment. In control (control), MMP-9 was stored within cells and also secreted to culture medium. In LPS-treated cells (LPS), MMP-9 was significantly decreased within cells and increased in culture medium. In donepezil-pretreated and LPS-treated cells (DPZ/LPS), MMP-9 within both cells and medium were as low as undetectable level. The expression of α-tubulin was shown as an internal control. #, *P<0.01* versus control. ##, *P<0.01* versus LPS. *, *P<0.05* versus control. (b) Gelatin zymography for analysis of MMP-9 enzymatic activity. Compared to control (control), proteinase activity of MMP-9 secreted to culture medium was significantly high in LPS-treated cells (LPS) and low in donepezil-pretreated and LPS-treated cells (DPZ/LPS). #, *P<0.01*.
doi:10.1371/journal.pone.0020629.g003

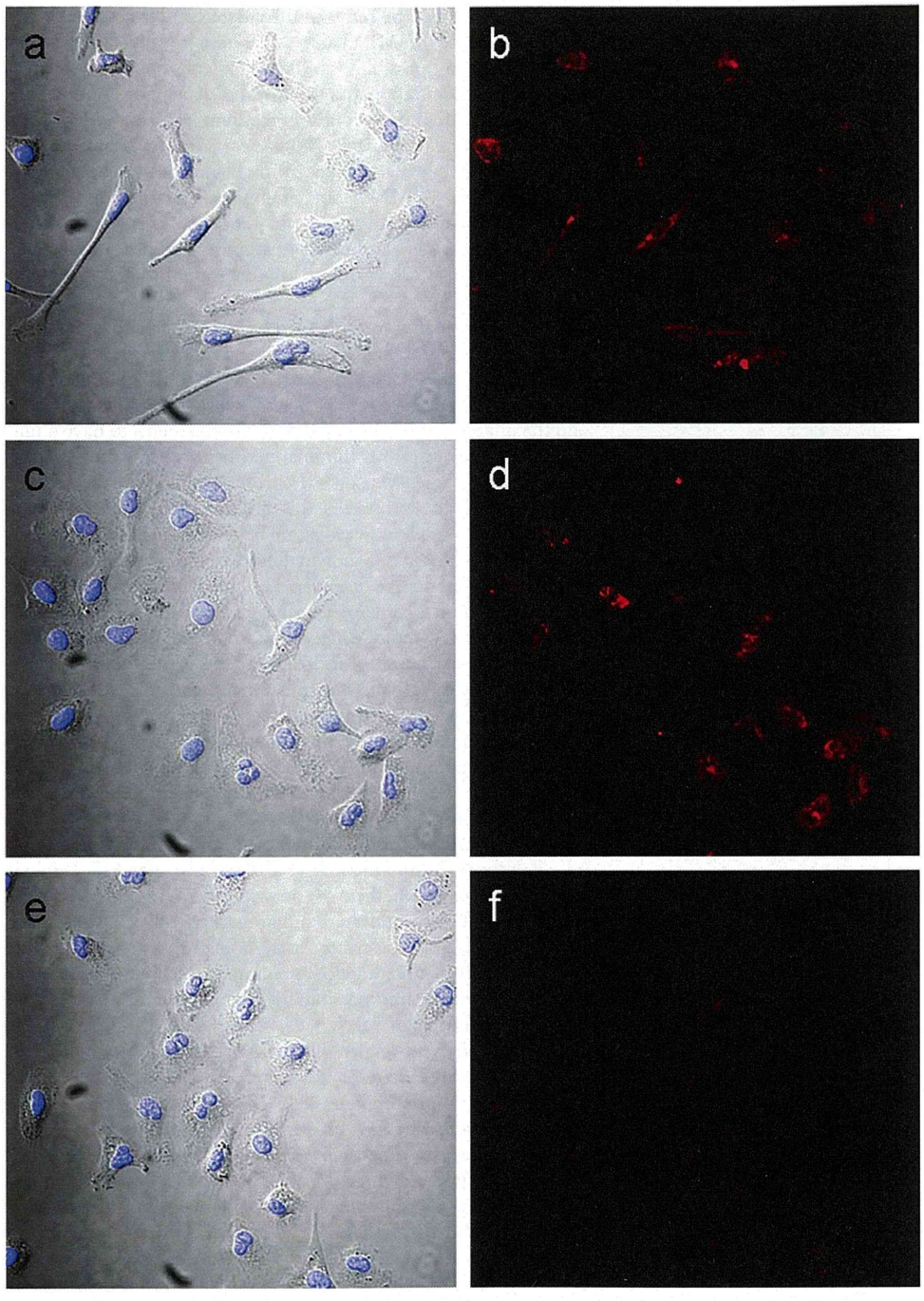

Figure 4. Immunocytochemistry with anti MMP-9 antibody in macrophages. DIC images showed that control macrophages had a spindle shape (a), whereas LPS-treated macrophages had a relatively round shape and numerous intracellular vacuoles regardless of donepezil pretreatment (c and e). Immunofluorescence micrographs showed that MMP-9 signals were observed around cytoplasm in the control (b) and the LPS-treated cells (d), which was lowered to undetectable levels by donepezil pretreatment (f).
doi:10.1371/journal.pone.0020629.g004

ACh have been shown to 1) prevent the loss of functional gap-junction channels and protect hearts against ischemia-induced lethal arrhythmias [4], 2) protect cardiomyocytes against hypoxia through the PI3K/Akt/HIF-1α pathway [5], 3) keep cell-cell communication by preserving the gap-junction protein level during hypoxia through inhibition of the connexin 43 degradation pathway [34], and 4) prevent a reperfusion-induced collapse in mitochondrial transmembrane potential by inhibition of mitochondrial permeability transition pore opening [35]. In the present study, to test whether or not an acetylcholinesterase inhibitor donepezil reproduced the cardioprotective effect of the vagal stimulation or ACh, we investigated the effect of donepezil on

Table 1. Physiological characteristics in sham operated and infarcted mice at 3 days after MI.

	sham	infarcted	
		untreated	DPZ
n	6	9	9
HR (bpm)	493±70	548±53	528±43
SBP (mmHg)	98.9±5.0	81.6±7.4 #	78.3±7.9 #
n	7	11	11
HW/BW (mg/g)	4.31±0.25	5.85±0.66 #	5.60±0.39 #

Values are means ± SD. HR, heart rate; SBP, systolic blood pressure; HW/BW, heart weight to body weight ratio; DPZ, donepezil-treated group. #, *P<0.01* versus sham group.
doi:10.1371/journal.pone.0020629.t001

inflammatory response and mortality after MI. As a result, it was shown that donepezil inhibits macrophage MMP-9 and reduces the risk of cardiac rupture during the acute phase of MI. These findings, taken together with our earlier studies [13–15], indicate that donepezil would be a novel pharmacotherapeutic drug for heart failure patients.

Murine MI is a good model for exploration of the molecular processes of ischemia-induced tissue injury, because the post-infarct inflammatory response shares common characteristics with higher mammalian species [36] and the murine ventricular free wall often ruptures within a week after the onset of MI, like humans [24,37,38]. The postinfarct inflammation has been recognized as an important feature of the cardiac remodeling after MI. A number of studies have reported that MMPs play important roles in the left ventricular remodeling, and inhibiting the enzymatic activity of MMPs prevented the progress of cardiac dysfunction and improved survival following MI [26,29,39]. Among the members of MMP family, MMP-9 seems to be a key enzyme in early myocardial remodeling and fatal cardiac rupture during an acute phase of MI [25,27]. After the onset of MI, macrophage infiltrates into infarcted myocardium and expresses MMP-9 to degrade extracellular matrix [40,41]. The present study demonstrated that, in *in vitro* study, donepezil inhibited MMP-9 in LPS-treated macrophages (Figures 1, 2, 3, 4) and that, in *in vivo* study, donepezil attenuated the inflammatory cell infiltration into the infarcted myocardium and decreased the expression and the enzymatic activity of MMP-9 at the infarct area (Figure 7), thereby reduced the risk of cardiac rupture during the acute phase of MI (Table 3). These results indicate that donepezil is a possible candidate agent for affecting the postinfarct inflammation and the extracellular matrix remodeling. Macrophage MMP-9 in culture medium was not affected by coincubation with donepezil (100 μM) at 37°C for 3 hrs (data not shown), suggesting that donepezil might not possess degradation activity toward MMP-9 but attenuate macrophage MMP-9 protein expression through certain receptors not yet identified. To clarify a donepezil-binding receptor and an intracellular signaling pathway downstream of the receptor, a future study should be conducted.

Table 2. Histological analysis in heart sections at 3 days after MI.

		untreated	DPZ
n		5	5
Wall thickness	left ventricle (μm)	68.7±10.7	89.8±21.5
	septum (μm)	134.6±13.1	132.0±6.2
	left ventricle/septum	0.51±0.07	0.69±0.20 ##
	right ventricle (μm)	56.1±8.91	43.9±7.31 ##
Infarct size (%)		68.3±3.12	62.6±9.61
Nuclear density ($\times 10^3/mm^2$)		4.42±0.36	3.50±0.29 #

Values are means ± SD. DPZ, donepezil-treated group. #, *P<0.01*. ##, *P<0.05*.
doi:10.1371/journal.pone.0020629.t002

Histological analysis on infarcted heart sections showed that left ventricular wall thinning and right ventricular hypertrophy were attenuated in the donepezil-treated group (Table 2), however, without significant differences of the heart to body weight ratio and the infarct size, suggesting that donepezil seems to have a mild anti-remodeling effect on the infarcted heart at this time point (3 days postinfarction). Masson's trichrome staining on the hearts 3 days after MI also supported this result, because collagen fibers were not distributed and cardiac myocytes still existed throughout the infarct area (data not shown). These observations indicate that the extracellular matrix turnover, i.e., the synthesis and degradation of collagen, to replace necrotic cardiomyocytes has not yet occurred, and LV remodeling would progress later. Nevertheless, in this study, cardiac rupture occurred frequently within 4 days after the onset of MI, and donepezil treatment reduced the risk of the lethal event. When ruptured, the wall perforation tended to occur at the infarct border zone (Figures 5c and d) where a large number of inflammatory cells invaded (Figure 6b). The number of inflammatory cells at the area was significantly lower in the donepezil-treated group than the untreated group (Table 2), indicating that donepezil attenuated the infiltration of the inflammatory cells into the infarct border zone after MI. Although it is still unclear whether or not donepezil inhibited MMP-9 production of the infiltrated inflammatory cells at the infarct border zone, it is conceivable that donepezil exerted the anti-rupture effect by inhibiting the inflammatory cell infiltration at the infarct border zone and possibly by retaining the local strength of the infarct ventricular wall.

In this study, the expression of MMP-9 mRNA in the left ventricular infarct area at 3 days after MI was reduced by donepezil in approximately half compared with that in the untreated group, whereas this was not accurately reflected in the protein level at this time point (Figures 7a and b). This might be due to the time difference in the process of transcription to translation, i.e., the inhibitory effect of donepezil on the de novo synthesis of MMP-9. In any case, the donepezil-treated mice showed a significantly lower incidence of cardiac rupture than the untreated mice (Table 3), accompanied by a reduced expression and enzymatic activity of MMP-9 in the left ventricular infarct area (Figure 7). Further studies are required to elucidate whether or not donepezil has effect on other types of MMP family members such as MMP-2 and MMP-13, and on their endogenous inhibitors, tissue inhibitor of matrix metalloproteinases (TIMPs). The effects of donepezil on the other cells including neutrophils, another source of MMP-9 [42], and cardiomyocytes should also be investigated.

Chronic effect of donepezil on ischemic heart failure has been also investigated in rats, demonstrating that donepezil improved the long-term survival through the prevention of postinfarct ventricular dysfunction and cardiac remodeling [13,43,44]. Although cardiac rupture has not so far been reported in rat models with MI as well as other laboratory

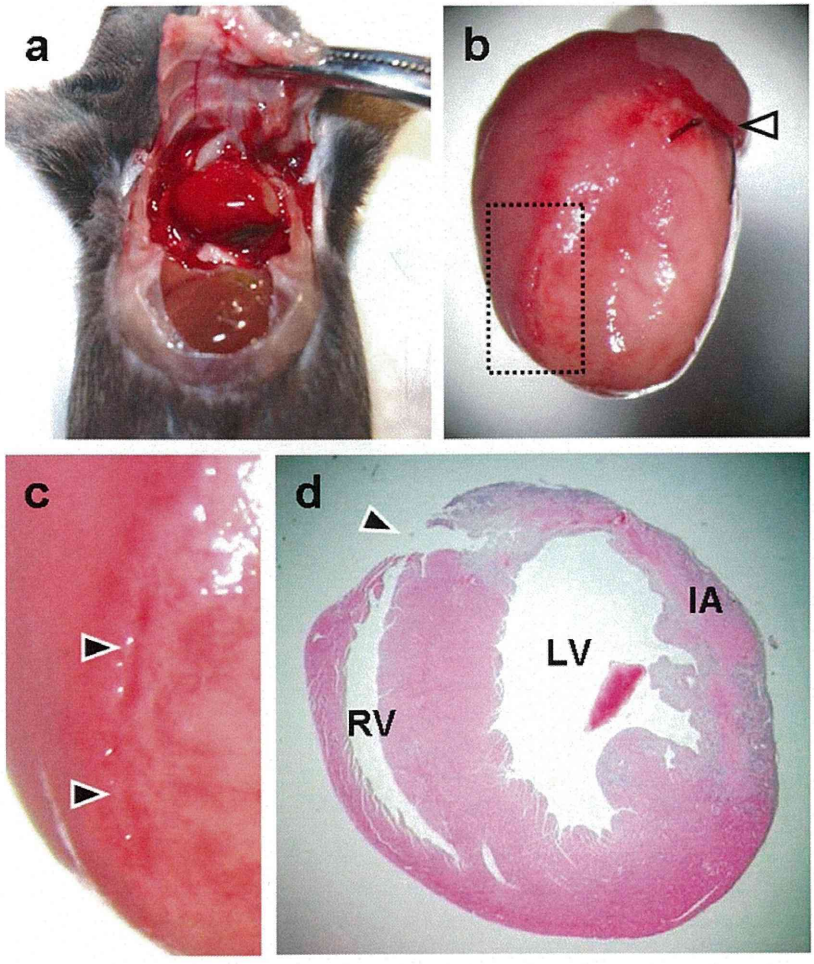

Figure 5. Light micrographs of an autopsied mouse that died due to cardiac rupture. (a) An infarcted mouse after the incidence of cardiac rupture. The chest cavity was filled with a large amount of clotted blood surrounding the heart. (b) The heart excised from the mouse. The ischemic area was visually identified by the pale myocardium. A white arrowhead represents the position of the coronary artery ligation. (c) An enlarged micrograph of the area shown by the small rectangle with a broken line in (b). A left ventricular perforation tends to occur at the border zone between infarcted and non-infarcted myocardium (black arrowheads). (d) The ruptured heart sectioned at a middle part of the left ventricular infarct area. The tissue was stained with hematoxylin and eosin. A black arrowhead shows the position of wall perforation occurred at left ventricular infarct border zone. RV, right ventricle; LV, left ventricle; IA, infarct area.
doi:10.1371/journal.pone.0020629.g005

animals, such as rabbits, dogs, pigs and sheep [45], pharmacological intervention of the MMPs attenuates the postinfarct remodeling [26,28,46,47]. Furthermore, donepezil pretreatment (100 μM) inhibited the LPS-induced increase of MMP-9 secretion even in rats macrophage (data not shown). Therefore, the inhibitory effect of donepezil on macrophage MMP-9 is also involved in protecting from rat cardiac remodeling during the acute phase of MI. Studies to determine the long-term effects of donepezil on inflammatory responses after MI are also needed.

Table 3. Cardiac rupture rate at 4 days after MI.

	sham	infarcted	
		untreated	DPZ
operated	6	49	46
ruptured	0	15	4
rupture rate (%)	0	30.6	8.7 #

DPZ, donepezil-treated group. #, $P<0.01$ versus untreated group.
doi:10.1371/journal.pone.0020629.t003

It is well known that a large dose of donepezil has a heart-rate slowing effect [48]. The dose of donepezil administrated to mice in the present study was approximately 50 times larger than the therapeutic doses used for Alzheimer's disease patients in clinical setting. However, the selected doses of donepezil lowered an incidence of cardiac rupture during acute phase of MI without slowing heart rate, indicating that the anti-rupture effect of donepezil was not brought by its bradycardiac action. Although the daily dose at 5.0 mg/kg has been extensively used in animal study with donepezil, it should be considered whether or not the clinical dose for donepezil also has a beneficial effect on heart failure comparably with the higher dose. It was shown that the oral administration of donepezil at dose of 0.5 mg/kg/day prevented the progression of left ventricular dysfunction on rat MI heart (unpublished data),

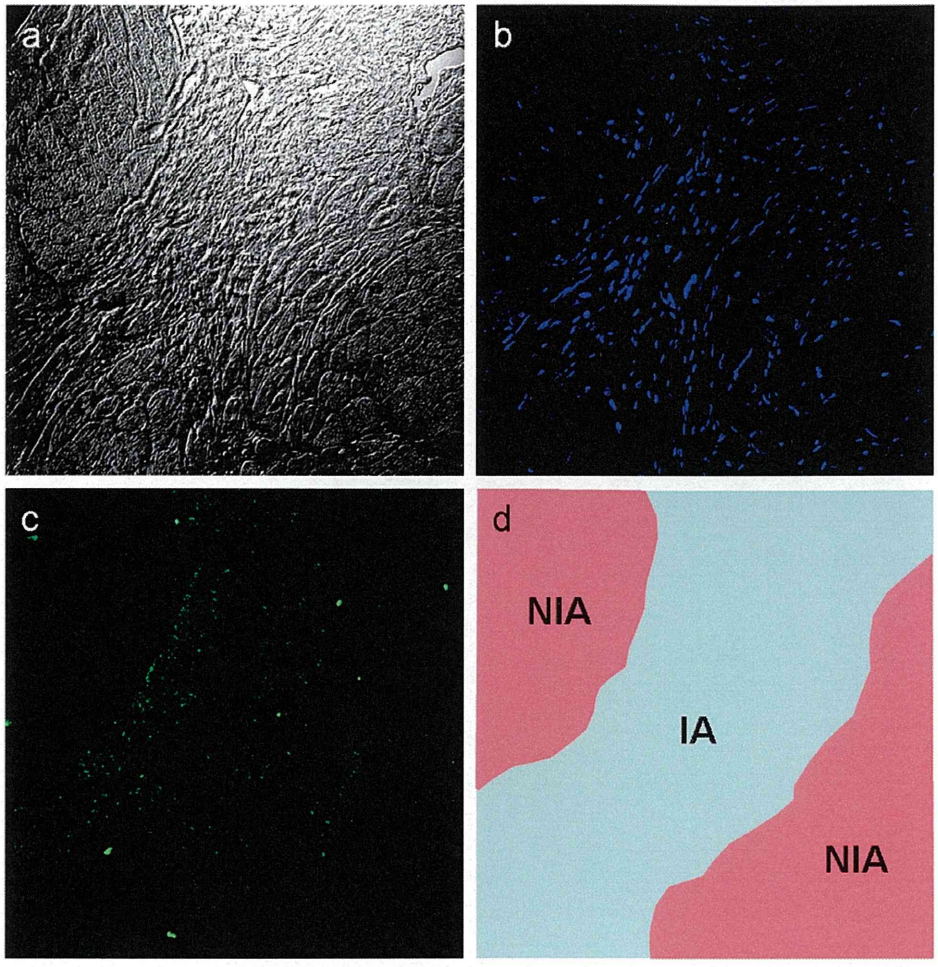

Figure 6. Immunohistochemistry of MMP-9 in infarcted myocardium. (a) A DIC image of the left ventricular infarct area. (b and c) The same fields stained with Hoechst 33258 to indicate the position of nuclei (b) and with a rabbit anti mouse MMP-9 antibody to indicate the localization of MMP-9 (c). (d) A schematic drawing of the field observed. IA and NIA represent infarct and non-infarct area, respectively.
doi:10.1371/journal.pone.0020629.g006

suggesting that donepezil at dose of 5.0 mg/kg/day is not necessarily required for the treatment of heart failure. Actually, our recent retrospective cohort study showed that donepezil-treated patients with Alzheimer's disease had reduced cardiovascular mortality [49].

It has been reported that the cholinergic anti-inflammatory pathway can directly modulate the systemic response through ACh by attenuating the release of inflammatory cytokines from macrophages. In the present study, donepezil inhibited MMP-9 expression in LPS-treated macrophages, but not tumor necrosis factor (TNF). The inhibitory effect of donepezil on macrophage MMP-9 could not be reproduced by ACh (Figure 2a) or other kinds of acetylcholinesterase inhibitors such as physostigmine and galanthamine (data not shown). Experimentally, ACh was shown to inhibit TNF release from LPS-stimulated macrophages [1], however, in our study, ACh failed to inhibit TNF release (data not shown). This discrepancy between our results and those of Borovikova et al. [1] might be derived from different cell sources and culture conditions. Moreover, neither a muscarinic ACh receptor blocker, atropine, nor a nicotinic ACh receptor blocker, mecamylamine, attenuated the inhibitory effect of donepezil on the MMP-9 release (Figure 2b). These results indicate that the specific characteristics of donepezil would be independent of its acetylcholinesterase inhibition. Recently accumulating evidence strongly suggests that donepezil possesses a direct cytoprotective activity, independent of its acetylcholinesterase-inhibitory mechanism [12,50–52]. Our previous study using an ischemic hindlimb model of α7 nicotinic receptor-deleted mice demonstrated the beneficial effect of donepezil on acceleration of angiogenesis, suggesting that donepezil rather exerts its specific effect independent of α7 nicotinic receptors [15]. Further studies focusing on the pharmacological properties of donepezil which directly affect cells via mechanism other than acetylcholinesterase inhibitory action are needed.

In summary, the results of the study reported here suggest that donepezil inhibits MMP-9 in macrophages which infiltrate into the infarcted myocardium, thereby contributes at least in part to the reduction of the risk in left ventricular free wall rupture during the acute phase of MI. Although donepezil is clinically used as a central type inhibitor of neural acetylcholinesterase, the donepezil-induced cardioprotection observed in this study may not be due to its pharmacological property of acetylcholinesterase inhibition. Understanding of the cellular and molecular mechanism of the donepezil-induced cardioprotection would help to establish a

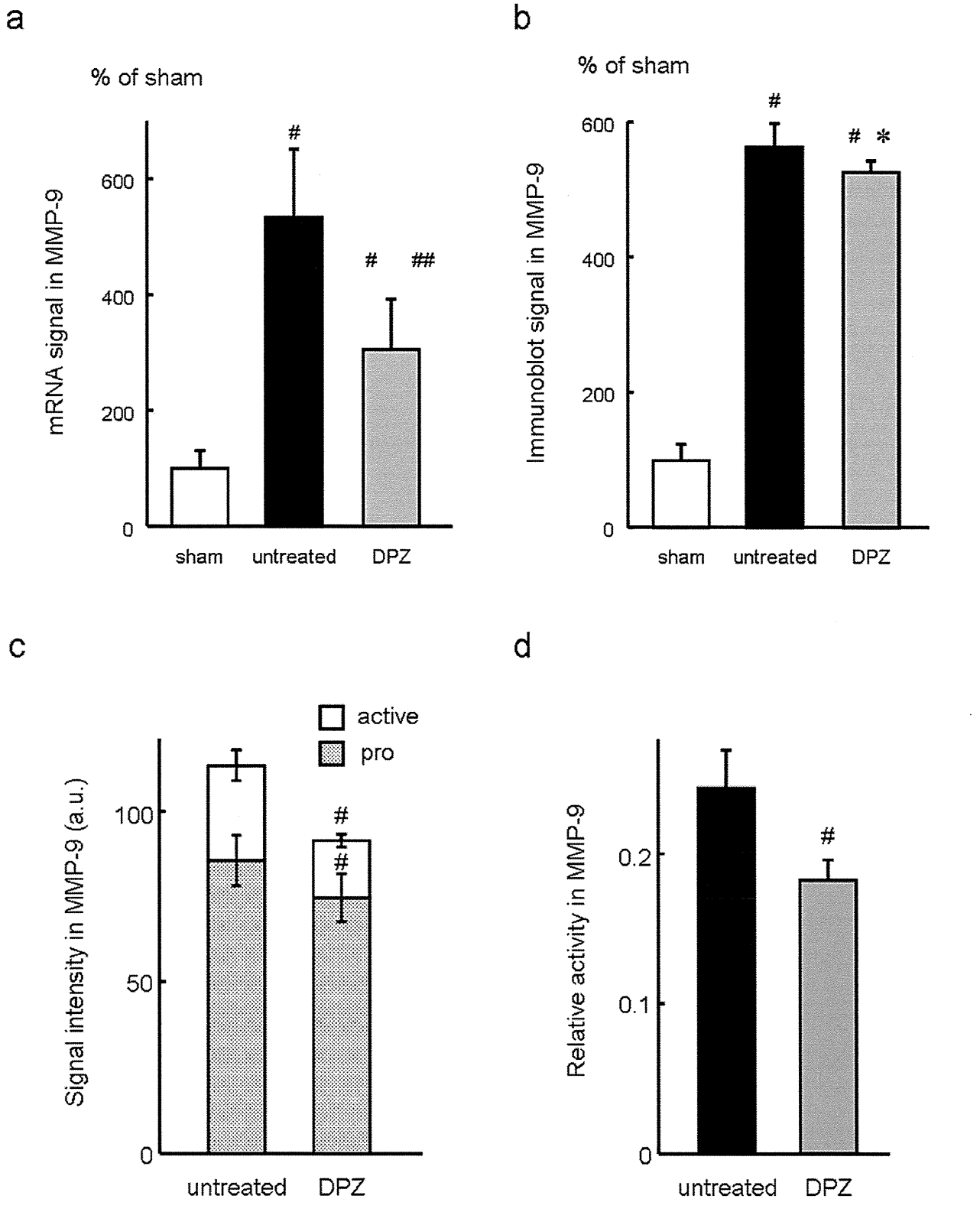

Figure 7. MMP-9 expression and its enzymatic activity in infarcted myocardium. MMP-9 expression in the left ventricular infarct area was compared among sham, untreated and donepezil-treated groups in mRNA (a) and protein level (b) at 3 days after myocardial infarction. (a) Compared to sham group (sham), MMP-9 mRNA in infarcted groups was significantly increased (untreated and DPZ). The increase of MMP-9 mRNA was significantly attenuated in the donepezil-treated group compared to the untreated group. #, $P<0.01$ versus sham group. ##, $P<0.01$ versus untreated group. (b) Compared to sham group (sham), MMP-9 protein in infarcted groups was significantly increased (untreated and DPZ). The increase of MMP-9 was slightly but significantly attenuated in the donepezil-treated group compared to the untreated group. #, $P<0.01$ versus sham

group. *, $P<0.05$ versus untreated group. Enzymatic activity of MMP-9 in the left ventricular infarct area was evaluated by gelatin zymography (c and d) at 3 days after myocardial infarction. (c) Compared to the untreated group (untreated), signal intensity in both pro and active forms of MMP-9 were significantly decreased in the donepezil-treated group (DPZ). #, $P<0.01$. (d) Relative activity (active/total MMP-9) was calculated and was significantly decreased in the donepezil-treated group (DPZ) compared to the untreated group (untreated). #, $P<0.01$.
doi:10.1371/journal.pone.0020629.g007

novel therapeutic strategy in the prevention and treatment against heart failure.

Acknowledgments

The authors acknowledge Mr. Ken-ichi Yagyu, Medical Research Center, Kochi Medical School, for the kind technical assistance in histology and immunohistochemistry.

Author Contributions

Conceived and designed the experiments: MA. Performed the experiments: MA. Analyzed the data: MA. Contributed reagents/materials/analysis tools: MA YK TH FY. Wrote the paper: MA YK TS. Discussed the results and commented on the manuscript: MA YK TH FY TS.

References

1. Borovikova LV, Ivanova S, Zhang M, Yang H, Botchkina GI, et al. (2000) Vagus nerve stimulation attenuates the systemic inflammatory response to endotoxin. Nature 405: 458–462.
2. Pavlov VA, Tracey KJ (2006) Controlling inflammation: the cholinergic anti-inflammatory pathway. Biochem Soc Trans 34: 1037–1040.
3. Li M, Zheng C, Sato T, Kawada T, Sugimachi M, et al. (2004) Vagal nerve stimulation markedly improves long-term survival after chronic heart failure in rats. Circulation 109: 120–124.
4. Ando M, Katare RG, Kakinuma Y, Zhang D, Yamasaki F, et al. (2005) Efferent vagal nerve stimulation protects heart against ischemia-induced arrhythmias by preserving connexin43 protein. Circulation 112: 164–170.
5. Kakinuma Y, Ando M, Kuwabara M, Katare RG, Okudela K, et al. (2005) Acetylcholine from vagal stimulation protects cardiomyocytes against ischemia and hypoxia involving additive non-hypoxic induction of HIF-1alpha. FEBS lett 579: 2111–2118.
6. Schwartz PJ, De Ferrari GM, Sanzo A, Landolina M, Rordorf R, et al. (2008) Long term vagal stimulation in patients with advanced heart failure: first experience in man. Eur J Heart Fail 10: 884–891.
7. Schwartz PJ, De Ferrari GM (2009) Vagal stimulation for heart failure: background and first in-man study. Heart Rhythm 6: S76–81.
8. De Ferrari GM, Sanzo A, Schwartz PJ (2009) Chronic vagal stimulation in patients with congestive heart failure. Conf Proc IEEE Eng Med Biol Soc. pp 2037–2039.
9. Whitehouse PJ, Struble RG, Clark AW, Price DL (1982) Alzheimer disease: plaques, tangles, and the basal forebrain. Ann Neurol 12: 494.
10. Ryan RE, Ross SA, Drago J, Loiacono RE (2001) Dose-related neuroprotective effects of chronic nicotine in 6-hydroxydopamine treated rats, and loss of neuroprotection in alpha4 nicotinic receptor subunit knockout mice. Br J Pharmacol 132: 1650–1656.
11. Donnelly-Roberts DL, Xue IC, Arneric SP, Sullivan JP (1996) In vitro neuroprotective properties of the novel cholinergic channel activator (ChCA), ABT-418. Brain Res 719: 36–44.
12. Takada Y, Yonezawa A, Kume T, Katsuki H, Kaneko S, et al. (2003) Nicotinic acetylcholine receptor-mediated neuroprotection by donepezil against glutamate neurotoxicity in rat cortical neurons. J Pharmacol Exp Ther 306: 772–777.
13. Okazaki Y, Zheng C, Li M, Sugimachi M (2010) Effect of the cholinesterase inhibitor donepezil on cardiac remodeling and autonomic balance in rats with heart failure. J Physiol Sci 60: 67–74.
14. Handa T, Katare RG, Kakinuma Y, Arikawa M, Ando M, et al. (2009) Anti-Alzheimer's drug, donepezil, markedly improves long-term survival after chronic heart failure in mice. J Card Fail 15: 805–811.
15. Kakinuma Y, Furihata M, Akiyama T, Arikawa M, Handa T, et al. (2010) Donepezil, an acetylcholinesterase inhibitor against Alzheimer's dementia, promotes angiogenesis in an ischemic hindlimb model. J Mol Cell Cardiol 48: 680–693.
16. Davis N, Sistino JJ (2002) Review of ventricular rupture: key concepts and diagnostic tools for success. Perfusion 17: 63–67.
17. Figueras J, Cortadellas J, Evangelista A, Soler-Soler J (1997) Medical management of selected patients with left ventricular free wall rupture during acute myocardial infarction. J Am Coll Cardiol 29: 512–518.
18. Purcaro A, Costantini C, Ciampani N, Mazzanti M, Silenzi C, et al. (1997) Diagnostic criteria and management of subacute ventricular free wall rupture complicating acute myocardial infarction. Am J Cardiol 80: 397–405.
19. McMullan MH, Maples MD, Kilgore TL, Jr., Hindman SH (2001) Surgical experience with left ventricular free wall rupture. Ann Thorac Surg 71: 1894–1898.
20. Leva C, Bruno PG, Gallorini C, Lazzarini I, Musazzi G, et al. (2006) Complete myocardial revascularization and sutureless technique for left ventricular free wall rupture: clinical and echocardiographic results. Interactive Cardiovasc Thorac Surg 5: 408–412.
21. Sakaguchi G, Komiya T, Tamura N, Kobayashi T (2008) Surgical treatment for postinfarction left ventricular free wall rupture. Ann Thorac Surg ; 85: 1344–1346.
22. Batts KP, Ackermann DM, Edwards WD (1990) Postinfarction rupture of the left ventricular free wall: clinicopathologic correlates in 100 consecutive autopsy cases. Hum Pathol 21: 530–535.
23. Fang L, Gao XM, Moore XL, Kiriazis H, Su Y, et al. (2007) Differences in inflammation, MMP activation and collagen damage account for gender difference in murine cardiac rupture following myocardial infarction. J Mol Cell Cardiol 43: 535–544.
24. Gao XM, Ming Z, Su Y, Fang L, Kiriazis H, et al. (2010) Infarct size and post-infarct inflammation determine the risk of cardiac rupture in mice. Int J Cardiol 143: 20–28.
25. Heymans S, Luttun A, Nuyens D, Theilmeier G, Creemers E, et al. (1999) Inhibition of plasminogen activators or matrix metalloproteinases prevents cardiac rupture but impairs therapeutic angiogenesis and causes cardiac failure. Nat Med 5: 1135–1142.
26. Rohde LE, Ducharme A, Arroyo LH, Aikawa M, Sukhova GH, et al. (1999) Matrix metalloproteinase inhibition attenuates early left ventricular enlargement after experimental myocardial infarction in mice. Circulation 99: 3063–3070.
27. Ducharme A, Frantz S, Aikawa M, Rabkin E, Lindsey M, et al. (2000) Targeted deletion of matrix metalloproteinase-9 attenuates left ventricular enlargement and collagen accumulation after experimental myocardial infarction. J Clin Invest 106: 55–62.
28. Lindsey ML, Gannon J, Aikawa M, Schoen FJ, Rabkin E, et al. (2002) Selective matrix metalloproteinase inhibition reduces left ventricular remodeling but does not inhibit angiogenesis after myocardial infarction. Circulation 105: 753–758.
29. Hayashidani S, Tsutsui H, Ikeuchi M, Shiomi T, Matsusaka H, et al. (2003) Targeted deletion of MMP-2 attenuates early LV rupture and late remodeling after experimental myocardial infarction. Am J Physiol 285: H1229–1235.
30. Matsumura S, Iwanaga S, Mochizuki S, Okamoto H, Ogawa S, et al. (2005) Targeted deletion or pharmacological inhibition of MMP-2 prevents cardiac rupture after myocardial infarction in mice. J Clin Invest 115: 599–609.
31. Pfeffer JM, Pfeffer MA, Fletcher P, Braunwald E (1979) Alterations of cardiac performance in rats with established spontaneous hypertension. Am J Cardiol 44: 994–998.
32. Pfeffer JM, Pfeffer MA, Braunwald E (1985) Influence of chronic captopril therapy on the infarcted left ventricle of the rat. Circ Res 57: 84–95.
33. Laemmli UK (1970) Cleavage of structural proteins during the assembly of the head of bacteriophage T4. Nature 227: 680–685.
34. Zhang Y, Kakinuma Y, Ando M, Katare RG, Yamasaki F, et al. (2006) Acetylcholine inhibits the hypoxia-induced reduction of connexin43 protein in rat cardiomyocytes. J Pharmacol Sci 101: 214–222.
35. Katare RG, Ando M, Kakinuma Y, Arikawa M, Handa T, et al. (2009) Vagal nerve stimulation prevents reperfusion injury through inhibition of opening of mitochondrial permeability transition pore independent of the bradycardiac effect. J Thorac Cardiovasc Surg 137: 223–231.
36. Dewald O, Ren G, Duerr GD, Zoerlein M, Klemm C, et al. (2004) Of mice and dogs: species-specific differences in the inflammatory response following myocardial infarction. Am J Pathol 164: 665–677.
37. Gao XM, Xu Q, Kiriazis H, Dart AM, Du XJ (2005) Mouse model of post-infarct ventricular rupture: time course, strain- and gender-dependency, tensile strength, and histopathology. Cardiovasc Res 65: 469–477.
38. Yang Y, Ma Y, Han W, Li J, Xiang Y, et al. (2008) Age-related differences in postinfarct left ventricular rupture and remodeling. Am J Physiol 294: H1815–1822.
39. Creemers EE, Cleutjens JP, Smits JF, Daemen MJ (2001) Matrix metalloproteinase inhibition after myocardial infarction: a new approach to prevent heart failure? Circ Res 89: 201–210.
40. Lindsey ML (2004) MMP induction and inhibition in myocardial infarction. Heart Fail Rev 9: 7–19.
41. Lambert JM, Lopez EF, Lindsey ML (2008) Macrophage roles following myocardial infarction. Int J Cardiol 130: 147–158.
42. Nagaoka I, Hirota S (2000) Increased expression of matrix metalloproteinase-9 in neutrophils in glycogen-induced peritoneal inflammation of guinea pigs. Inflamm Res 49: 55–62.

43. Arikawa M, Katare RG, Kakinuma Y, Handa T, Ando M, et al. (2007) Progression of ventricular dysfunction after myocardial infarction is prevented by anti-Alzheimer's disease drug, donepezil. Circulation 116: II_291.
44. Li M, Zheng C, Kawada T, Inagaki M, Sato T, et al. (2009) Donepezil markedly suppresses ventricular dysfunction and improves neurohumoral states on top of losartan in rats with extensive myocardial infarction. Circulation 120: S1178.
45. Fang L, Gao XM, Samuel CS, Su Y, Lim YL, et al. (2008) Higher levels of collagen and facilitated healing protect against ventricular rupture following myocardial infarction. Clin Sci (Lond) 115: 99–106.
46. Peterson JT, Hallak H, Johnson L, Li H, O'Brien PM, et al. (2001) Matrix metalloproteinase inhibition attenuates left ventricular remodeling and dysfunction in a rat model of progressive heart failure. Circulation 103: 2303–2309.
47. Spinale FG, Coker ML, Krombach SR, Mukherjee R, Hallak H, et al. (1999) Matrix metalloproteinase inhibition during the development of congestive heart failure: effects on left ventricular dimensions and function. Circ Res 85: 364–376.
48. Shepherd G, Klein-Schwartz W, Edwards R (1999) Donepezil overdose: a tenfold dosing error. Ann Pharmacother 33: 812–815.
49. Sato K, Urbano R, Yu C, Yamasaki F, Sato T, et al. (2010) The effect of donepezil treatment on cardiovascular mortality. Clin Pharmacol Ther 88: 335–338.
50. Takada-Takatori Y, Kume T, Ohgi Y, Izumi Y, Niidome T, et al. (2008) Mechanism of neuroprotection by donepezil pretreatment in rat cortical neurons chronically treated with donepezil. J Neurosci Res 86: 3575–3583.
51. Akasofu S, Kimura M, Kosasa T, Sawada K, Ogura H (2008) Study of neuroprotection of donepezil, a therapy for Alzheimer's disease. Chem Biol Interact 175: 222–226.
52. Akaike A, Takada-Takatori Y, Kume T, Izumi Y (2010) Mechanisms of neuroprotective effects of nicotine and acetylcholinesterase inhibitors: role of alpha4 and alpha7 receptors in neuroprotection. J Mol Neurosci 40: 211–216.

Surg Today (2011) 41:1467–1474
DOI 10.1007/s00595-010-4553-0

SURGERY TODAY

Review Article

Assessing Intraoperative Blood Flow in Cardiovascular Surgery

MASAKI YAMAMOTO[1], SHIRO SASAGURI[1], and TAKAYUKI SATO[2]

Departments of [1]Surgery II and [2]Cardiovascular Control, Faculty of Medicine, Kochi University, Kohasu, Oko, Nankoku, Kochi 783-8505, Japan

Abstract
Off-pump coronary arterial bypass grafting and new surgical apparatus and techniques have decreased the mortality rate associated with this procedure to approximately 1.5%. If we could detect problems in the constructed coronary anastomoses by an alternative imaging system to coronary angiography during surgery, decisions to revise the surgical procedure could be made without hesitation. Meanwhile, the intraoperative direct evaluation of intestinal blood flow during abdominal aortic aneurysmal surgery is required to prevent ischemic colitis, which is a devastating complication. Indocyanine green (ICG) has recently improved ophthalmic angiography and the navigation systems of oncological surgery. The fluorescence illumination of ICG with a near-infrared light is captured on camera. In coronary arterial surgery, the ICG imaging system is also becoming increasingly useful. A new ICG imaging system, the HyperEye Medical System (HEMS), provides a clear view of the blood flow and ischemic area with color visualization. Furthermore, its combination with a quantitative blood flow assessment tool such as transit time flow measurement could improve the accuracy of intraoperative examination. In this review, we evaluate the current strategies of assessing blood flow intraoperatively with an ICG imaging system in cardiovascular surgery.

Key words Intraoperative assessment of blood flow · Indocyanine green imaging system · Hyper Eye Medical System · Coronary artery bypass grafting · Transit time flow measurement

Reprint requests to: M. Yamamoto
Received: August 24, 2010 / Accepted: November 17, 2010

Introduction

Coronary artery disease (CAD) has becomes the leading cause of death in developed countries. Surgery for angina and myocardial ischemia began with the Veinberg operation in 1946: Nowadays, about 18000 patients undergo coronary artery bypass grafting (CABG) each year in Japan. It has been reported that improved techniques, such as off-pump coronary artery bypass grafting (OPCAB), arterial grafts, and new surgical devices, have reduced the mortality of elective CABG down to about 1.5%.[1–4] The decreased mortality can also be attributed to advances in off-pump CABG; however, their effectiveness is dependent on surgical technique.[2,5–7] An increasing tendency toward re-CABG for recurrent angina attributed to graft occlusion or stenosis has been reported.[2] Balacumaraswami et al. reported 943 graft failures among 4735 grafts (19.9%) in patients who underwent CABG.[8]

The patency of bypass grafts has been evaluated with the coronary artery graph (CAG) and computed tomography (CT), while transit time flow measurement (TTFM) has also been introduced as an effective device for the intraoperative evaluation of bypass grafts.[9] Imaging techniques that rival CAG are required to allow us to see constructed coronary anastomoses. If problems with constructed coronary anastomoses can be detected through imaging as well as CAG during surgery, it would enable us to make a decision on revising the surgical procedure immediately. Furthermore, surgeons conventionally believe that it is difficult to identify the buried coronary artery that could be used in CABG anastomoses. Therefore, a detection tool is needed so we can decide which target coronary arteries should be bypass grafted.

Intestinal ischemia is a devastating complication of abdominal aortic aneurysm (AAA) repair, associated with a 40%–48% mortality rate.[10–12] Previously, the intestinal blood flow was assessed intraoperatively by mea-

suring inframesenteric artery (IMA) stump pressure, transanal Doppler ultrasound, and near-infrared spectroscopy. Ernst et al. prospectively studied the correlation between distal IMA stump pressure and ischemic colitis.[10] Ischemic colitis may develop after IMA or internal iliac artery (IIA) reconstruction.[12–14] The incidences of ischemic colitis after elective AAA surgery and AAA rupture are reported to be 6% and 42%, respectively.[12,13] According to Piotrowski et al., preoperative shock is the most important predictor of colonic ischemia following ruptured AAA.[15] Champagne et al. reported on the mortality rates of bowel ischemia with colonoscopic findings.[13] Although reconstruction of the blood flow in at least one IMA and IIA is commonly performed to prevent ischemic colitis, there is little evidence to support the effectiveness of these methods. Therefore, the direct evaluation of intestinal blood flow is required. Iwai et al. evaluated the rectal ischemia of patients who underwent AAA surgery by fixing a transanal Doppler probe in the rectum to detect blood flow in the upper rectal arterial area.[16] Furthermore, skin perfusion of both buttocks was detected with near-infrared spectroscopy. Visual evaluation of the intestinal blood flow intraoperatively allows us to decide on the need for reconstruction of the IMA or IIA in real time.

The incidence of peripheral artery occlusive disease (PAD) is increasing, for which catheter-based therapy is continually improving. The effectiveness of catheter-based therapy for PAD was demonstrated in a recent Bypass versus Angioplasty in Severe Ischemia of the Leg (BASIL) trial.[17] In the era of interventional surgery for PAD, the number of patients with critical limb ischemia requiring surgical therapy is substantially increasing. Although patients with the most advanced critical limb ischemia (CLI) should be given the choice of undergoing bypass involving either the tibial artery or the dorsal artery with saphenous vein grafts, anastomosis is often performed, despite the difficulties involved, because of the poor condition of the arteries.[17] It is common practice to evaluate the bypass graft with a portable X-ray fluoroscope or flowmetry during the operation. However, the use of conventional X-ray fluoroscope systems is associated with difficulties, such as complicated X-ray apparatus and establishing a line for angiography. Moreover, patients with chronic renal failure can suffer radiocontrast-induced renal failure. Technical errors when performing a bypass graft may necessitate lower limb amputation, limiting activities of daily living; therefore, a more reliable intraoperative imaging tool is required.

Intraoperative Imaging Techniques

Postoperative CAG and multidetector CT allow for visualization of anastomoses at a high resolution. Although these imaging tools enable us to detect problems with the graft postoperatively, it is too late to revise the graft anastomoses. Conversely, if the bypass graft patency and quality of anastomosis could be assessed intraoperatively, graft revision may be possible. Intraoperative indocyanine green (ICG) angiography would resolve this problem.[18–20]

Indocyanine Green Imaging

Indocyanine green is a hydrophilic tricarbocyanine dye that rapidly binds to plasma proteins in the body. It has been used for testing liver function and in ophthalmic angiography.[21] The fluorescence properties of ICG emit a flash of light with a wavelength of 806 nm, although our preliminary study showed that the peak spectral absorption for ICG diluted in human blood was 760–780 nm.[22] Water and hemoglobin have light absorption properties within organs. The fluorescence illuminated with near-infrared laser light or light-emitting diode (LED) light is captured on a charge-coupled device (CCD) video camera. Indocyanine green fluorescence illumination can be captured to a depth of less than 1 mm, allowing the visualization of blood flow in superficial tissues. The effectiveness of ICG angiography in fluorescein fundus angiography has improved the visualization of retinal and choroidal circulation.[23,24] The allergy-related reaction of ICG is dose dependent, being highest at a dose of more than 0.5 mg/kg body weight. This allergy-related reaction has been reported to occur at an incidence of approximately 1:40 000.[25]

Several reports have described a novel method of using ICG imaging to identify sentinel nodes with high sensitivity in breast and gastroenterological cancer.[26–28] In cardiovascular surgery, the value of intraoperative ICG imaging is being reported increasingly.[18,22,29,30] The commercialized SPY imaging system (Novadaq Technologies Inc., Toronto, Canada) is based on the fluorescence of ICG. The radiation of the SPY utilizes a low-intensity laser with a total output of 2.2 W spread over an area of 7.5 × 7.5 cm at a distance of 30 cm, which eliminates the risk of thermal injury.[29] In surgery, the articulating arm is covered with a sterile drape and after injecting ICG, the laser is activated and the image is acquired. A new ICG imaging system, the Photodynamic Eye (PDE; Hamamatsu Photonics K. K., Shizuoka, Japan), has been developed, which allows for imaging in the surgical field by using a hand-held camera. The PDE system is a simpler, more mobile, and improved version of the ICG imaging system.

HyperEye Medical System

We previously described a new ICG imaging system (HyperEye Medical System; HEMS, Mizuho Ikakogyo CO., Ltd, Japan) that consists of optical filters and an ultrahigh-sensitive color CCD imaging camera with

non-Bayer color filter arrays (HyperEye Technology; United States Patent Application 20080251694), which can detect visible and near-infrared rays from 380 to 1200 nm with no bias in the color balance, at 30 frames per second[22,31] (Fig. 1). Excitation of ICG is induced with an LED (760 nm) light source in the HEMS imaging system. The CCD camera is positioned about 30–50 cm above the surgical site. The focus, iris, and range are remote-controlled, thus ensuring that the camera is in a free position, and ICG dye is injected into the patient via a central venous catheter. The usual dose of ICG administered is 2.5 mg per image sequence. The video is recorded and stored immediately in AVI format, although the monochrome visualization of conventional ICG imaging cannot provide a surgical view on the monitor before the ICG injection. HEMS provides a different color image to conventional ICG imaging (Fig. 2). The color imaging recognizes the advantage of a navigation system in the orientation of the coronary arteries. Furthermore, in conventional ICG imaging that uses a laser light source, irradiation cannot be delivered for more than 35 s because of the danger of thermal injury. By contrast, the HEMS system provides color imaging without the problem of a limited irradiation time, by using LED.[22]

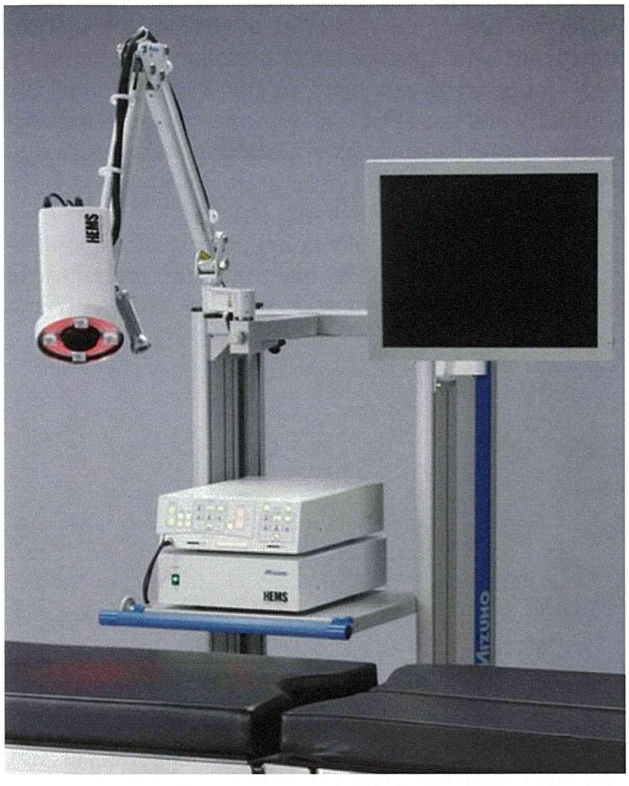

Fig. 1. The HyperEye Medical System (HEMS) consists of LED lights and an ultrasensitive color charge-coupled device (CCD) camera, which can visualize the optical wavelengths and near-infrared rays from 380 to 1200 nm

Transit Time Flow Measurement

Transit time flow measurement (TTFM) is based on the principle of transit time ultrasound technology.[32] The time it takes for ultrasound beams sent by an ultrasound wave to travel from one crystal across a vessel to the another crystal is called "transit time".[29,32] Blood flow such as that measured in a coronary arterial bypass graft, is rated by TTFM based on mean graft flow (MGF), pulsatility index (PI), and diastolic filling percentage (DF).[32–34] D'Ancona et al. explained that mean arterial blood pressure and graft coronary resistance influence mean flow.[32,33] They found that certain physical factors, such as blood viscosity, graft length, and graft radius, affect the aforementioned parameters.[32,33] Having studied the normal presented transit time patency criteria, the authors have set the following classification criteria, based on previous descriptions:[22]

Normal: mean flow >10 ml/min; PI <5; and DF >50%
Abnormal: mean flow <10 ml/min; PI >5; or DF <50%

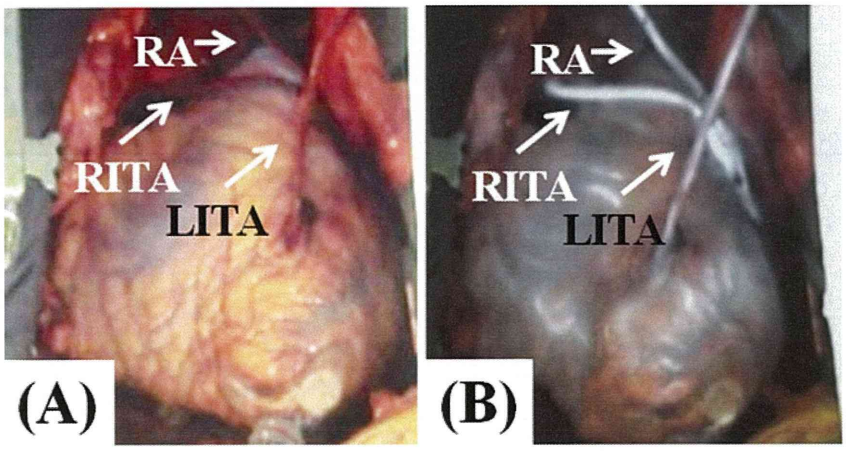

Fig. 2A,B. HEMS Indocyanine green (ICG) imaging shows the bypass graft and coronary arteries. The in situ left internal thoracic artery (*LITA*) was anastomosed to the left anterior descending artery, the right internal thoracic artery (*RITA*) was anastomosed to the diagonal branch, and the radial artery (*RA*) graft was anastomosed to the posterolateral coronary artery. **A** Pre-ICG imaging with a color-scale CCD HEMS. **B** The color-scale ICG imaging

If there is no quantifiable flow, a graft is deemed to be occluded.

Application of ICG Imaging in Cardiovascular Surgery

Usability of the ICG Imaging System in CABG

Since we can use the ICG imaging technique to assess the quality of coronary anastomoses visually, it allows us to decide on the need to revise anastomoses in real time (Fig. 3). Conversely, the prognosis of patients who do not undergo graft revision worsens if ICG imaging is not able to be done.[29] Other investigators have reported the reliability of intraoperative ICG imaging in clinical and experimental studies on CABG (Table 1). The first reported trial of intraoperative ICG imaging in coronary artery surgery was by Rubens et al. in 2002.[21] Reuthebuch et al.[19] and Taggart et al.[20] subsequently showed the clinical utility of the SPY system for assessing the quality of bypass grafts based on their experience. Takahashi et al. described the verification of ICG angiography by using the SPY imaging system.[18] In their study, the SPY system revealed four grafts problems among a collective 290 grafts in 72 off-pump CABG patients. Desai et al. researched the utility of two intraoperative graft assessment techniques: TTFM and ICG graft angiography.[35] They reviewed 139 grafts, and confirmed the sensitivity and specificity of ICG angiography by revealing that it detected greater than 50% stenosis or occlusion in 83.3% and 100%, respectively.[35] We have reported the reliability of ICG angiography as compared with postoperative coronary angiography. Fifth grafts were examined in this research, and the sensitivity and specificity of ICG angiography to detect greater than 50% stenosis or occlusion were 100% and 100%, respectively.[22] Revised graft anastomoses comprised 1.4% of all grafts in our research.

While ICG angiography could not provide quantitative measurements, TTFM quantified the graft flow in terms of certain parameters, such as MGF, PI, and

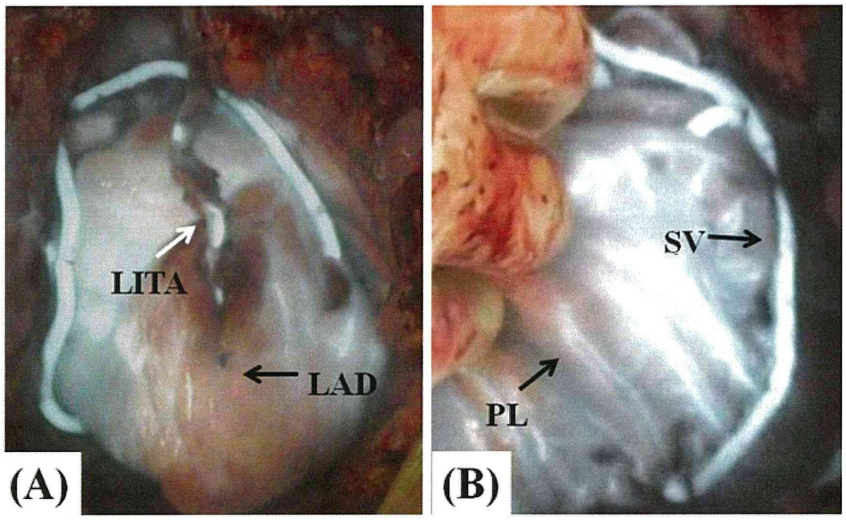

Fig. 3A,B. HEMS ICG imaging shows occlusion of the anastomosis of the left internal thoracic artery (*LITA*) graft to the left anterior descending artery (*LAD*). **A** No fluorescence was seen in the LITA graft to the LAD. There was no dye in the anterior wall of the left ventricle (the perfusion area of the LAD). **B** No fluorescence was seen in the saphenous vein (*SV*) graft to the posterolateral (*PL*) branch

Table 1. Reported clinical studies on the indocyanine green imaging system in coronary artery bypass grafting

First author[Ref.]	Year	Patients	No. of grafts	Sensitivity	Specificity
Rubens[21]	2002	20	—	—	—
Reuthebuch[19]	2003	38	124	—	—
Taggart[20]	2003	84	213	—	—
Balacumaraswami[29]	2004	200	533	—	—
Takahashi[18]	2004	72	290	—	—
Desai[35]	2006	46	139	83.3	100
Handa[22]	2009	39	116	100	100
Handa[31]	2010	51	129	85.7	100

—, not shown

DF.[8,19,32] The results of the intraoperative examination of TTFM have been documented by several institutions.[7,9,22,35,36] The results of clinical trials by Desai et al. showed that the sensitivity and specificity of TTFM in detecting greater than 50% stenosis or occlusion were 25% and 98.4%, respectively.[35] Hirotani et al. reported the utility of TTFM versus postoperative angiography.[7] In reviewing the clinical value of TTFM to assess graft patency, Balacumaraswami et al. reported that overall, 3.2% of 1411 grafts in 8.8% of 509 patients were revised according to TTFM findings.[29] However, based on their clinical studies, Balacumaraswami et al. suggested that TTFM findings alone may prompt unnecessary graft revision. D'Ancona et al. determined whether TTFM could be used to evaluate coronary graft patency in 409 patients who underwent CABG.[9] Of 1145 grafts, 37 (3.2%) were revised, 34 (3.0%) of which were revised for both low and abnormal flow curve patterns. In our recent studies, TTFM showed 5 competitive grafts among 116 grafts, although postoperative CAG showed that all the grafts were patent.[22,31] By contrast, CAG indicated graft failure in four grafts despite a normal flow pattern of TTFM, resulting in the sensitivity of TTFM being 93%.[22] Several intraoperative assessment modalities have been reported, including TTFM and ICG imaging, but it would not be possible to compare the advantages of ICG imaging and TTFM as their characteristics and methods are so different. Some investigators have compared the sensitivity and specificity of

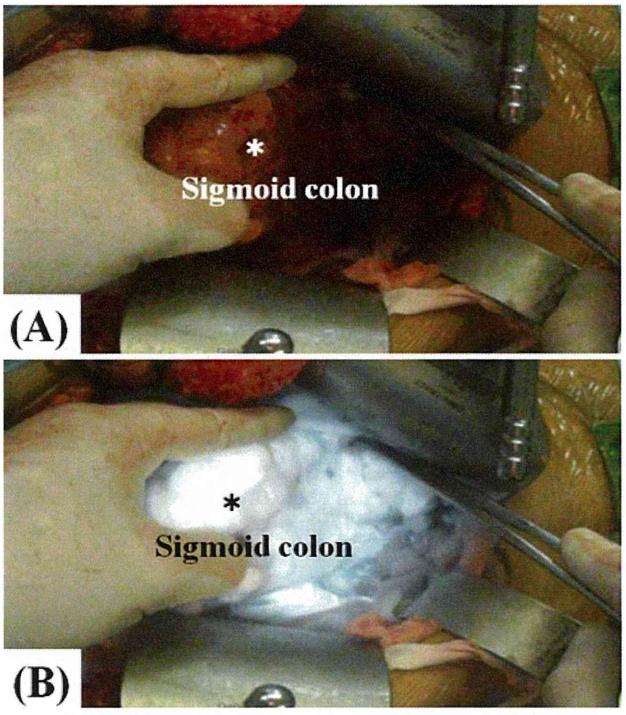

Fig. 4A,B. Indocyanine green fluorescence of the sigmoid colon (*asterisk*) in abdominal aneurysm surgery by HEMS ICG imaging. **A** Pre-ICG imaging of the sigmoid colon with a color-scale CCD camera. **B** Color-scale ICG imaging of the sigmoid colon

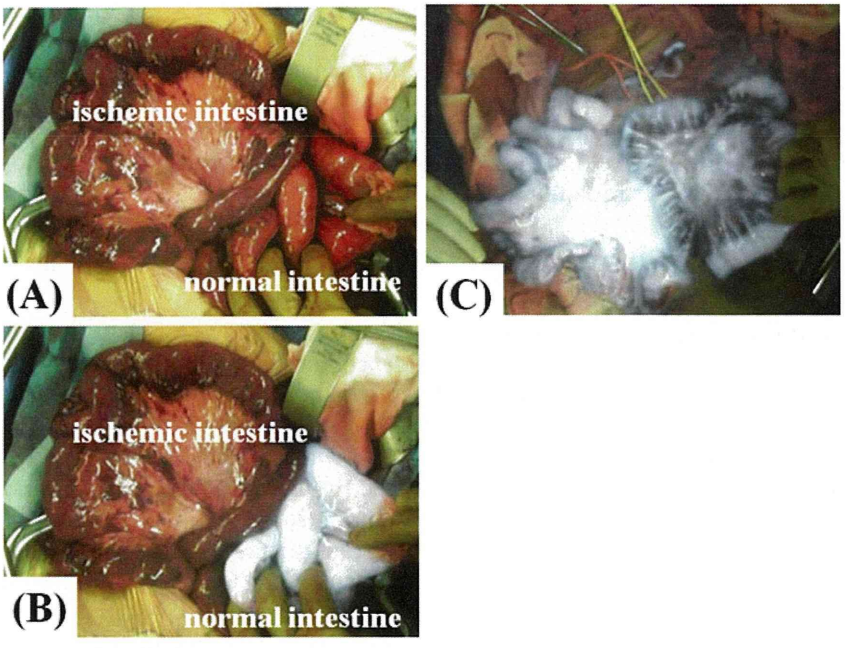

Fig. 5A–C. HEMS imaging showing intestine in the abdominal surgery. **A** Pre-ICG imaging with a color-scale CCD camera. **B** No fluorescence was seen in the ischemic intestine in the contrast of normal intestine. **C** After thrombectomy of the superior mesenteric artery, ICG imaging shows fluorescence in the reperfused intestine

ICG imaging with those of TTFM, but this comparison may not be useful. Indocyanine green imaging and TTFM are dependent to some degree on systemic blood pressure, cardiac output, hematocrit level, the variety and caliber of graft types, perfusion area, and ICG dosage. Therefore, these intraoperative assessment tools are unable to completely analyze the graft flow quantitatively. Both ICG imaging and TTFM can be used as intraoperative tools to assess graft flow in CABG. We believe that surgeons have no objection to either the use of or the comprehensive assessment of either tool.

Application in Vascular Surgery

By being able to visually assess intestinal blood flow intraoperatively, the need to reconstruct intestinal blood flow can be determined in real time. Indocyanine green imaging has been used to assess procedures for local perfusion in AAA surgery, similarly to the graft imaging used in CABG. In our study, HEMS color imaging allowed visualization of the ischemic area of the colon or intestine (Fig. 4). In principle, bilateral IIAs are reconstructed in our surgical strategy and IMA stump pressure is quantitatively evaluated in accordance with Ernst's procedure.[10] After this classical procedure, blood flow in the intestine and colon is confirmed by ICG imaging. HEMS color imaging allows us to pinpoint the exact location of the ischemic colon and the colored view helps us predict the obstruction point (Fig. 4). Moreover, abdominal organ ischemia is detected in real time during abdominal surgery, which is not the same as AAA surgery. We have experienced patients with a superior mesenteric arterial embolism. HEMS imaging allows us to detect the ischemic intestinal lesion and the thrombosed superior mesenteric artery (SMA) and its branches (Fig. 5). It also enables us to delineate the extent of ischemia from more than just a megascopic view.

Application in Peripheral Arterial Surgery

Digital subtraction angiography (DSA) with a portable X-ray machine is used for intraoperative imaging in peripheral arterial surgery. A mobile imaging system is also used for intraoperative imaging in PAD surgery. Unno et al. reported the clinical practicality of ICG imaging for assessing lower leg bypass with the PDE system in nine patients with CLI who underwent a distal bypass grafting.[37] ICG imaging using the PDE system showed that case graft revision was required in one patient when the initial bypass did not show any fluorescence signals at the distal anastomosis. We examined a CLI patient who underwent paramalleolar artery bypass. HEMS imaging showed a problem with the graft, and additional bypass grafting improved blood flow (Fig. 6).

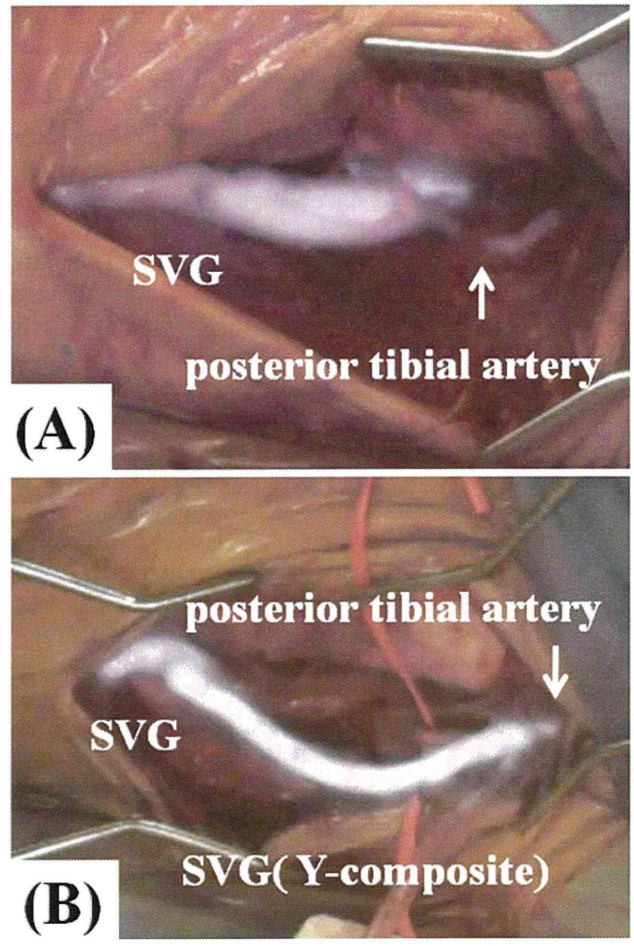

Fig. 6A,B. Indocyanine green imaging of a saphenous vein graft (*SVG*) in posterotibial arterial bypass. There was a lack of fluorescence in the posterior tibial artery

Indocyanine green imaging is useful in peripheral arterial surgery to assess graft patency quickly, with a high level of confidence. There is a great need for handheld ICG imaging systems, such as the PDE system, for broad-area imaging.

Conclusion

The ICG imaging system, which allows for visualization, has improved confidence in cardiovascular surgery and is used for graft assessment intraoperatively at many facilities. The HEMS allows the surgeon to see the blood flow clearly. If problems with constructed graft anastomoses can be evaluated through this type of imaging as well as angiography during surgery, decisions to revise the surgical procedure can be made without hesitation. Thus, in cardiovascular surgery, ICG imaging is a useful tool for evaluation of not only the coronary artery bypass, but also intestinal blood flow and the peripheral

arteries. It also enables us to detect signs of organ ischemia in real time. One of its limitations is that it cannot provide a quantitative evaluation of graft flow; however, TTFM allows for good quantitative assessment intraoperatively. Thus, the combination of ICG imaging and TTFM should be used for evaluation in cardiovascular surgery.

Acknowledgments. This study was supported by a grant for Science and Technology Incubation Program in Advanced Regions from the Japan Science and Technology Agency.

References

1. Parolari A, Alamanni F, Polvani G, Agrifoglio M, Chen YB, Kassem S, et al. Meta-analysis of randomized trials comparing off-pump with on-pump coronary artery bypass graft patency. Ann Thorac Surg 2005;80:2121–5.
2. Khan NE, De Souza A, Mister R, Flather M, Clague J, Davies S, et al. A randomized comparison of off-pump and on-pump multivessel coronary-artery bypass surgery. N Engl J Med 2004;350:21–8.
3. Puskas JD, Williams WH, Mahoney EM, Huber PR, Block PC, Duke PG, et al. Off-pump vs conventional coronary artery bypass grafting: early and 1-year graft patency, cost, and quality-of-life outcomes: a randomized trial. JAMA 2004;291:1841–9.
4. Shroyer AL, Grover FL, Hattler B, Collins JF, McDonald GO, Kozora E, et al. On-pump versus off-pump coronary-artery bypass surgery. N Engl J Med 2009;361:1827–37.
5. Puskas JD, Thourani VH, Marshall JJ, Dempsey SJ, Steiner MA, Sammons BH, et al. Clinical outcomes, angiographic patency, and resource utilization in 200 consecutive off-pump coronary bypass patients. Ann Thorac Surg 2001;71:1477–83; discussion 83–4.
6. Kobayashi J, Tashiro T, Ochi M, Yaku H, Watanabe G, Satoh T, et al. Early outcome of a randomized comparison of off-pump and on-pump multiple arterial coronary revascularization. Circulation 2005;112:I338–43.
7. Hirotani T, Kameda T, Shirota S, Nakao Y. An evaluation of the intraoperative transit time measurements of coronary bypass flow. Eur J Cardiothorac Surg 2001;19:848–52.
8. Balacumaraswami L, Taggart DP. Intraoperative imaging techniques to assess coronary artery bypass graft patency. Ann Thorac Surg 2007;83:2251–7.
9. D'Ancona G, Karamanoukian HL, Ricci M, Schmid S, Bergsland J, Salerno TA. Graft revision after transit time flow measurement in off-pump coronary artery bypass grafting. Eur J Cardiothorac Surg 2000;17:287–93.
10. Ernst CB, Hagihara PF, Daugherty ME, Griffen WO, Jr. Inferior mesenteric artery stump pressure: a reliable index for safe IMA ligation during abdominal aortic aneurysmectomy. Ann Surg 1978;187:641–6.
11. Chen JC, Hildebrand HD, Salvian AJ, Taylor DC, Strandberg S, Myckatyn TM, et al. Predictors of death in nonruptured and ruptured abdominal aortic aneurysms. J Vasc Surg 1996;24:614–20; discussion 21–3.
12. Champagne BJ, Lee EC, Valerian B, Mulhotra N, Mehta M. Incidence of colonic ischemia after repair of ruptured abdominal aortic aneurysm with endograft. J Am Coll Surg 2007;204:597–602.
13. Champagne BJ, Darling RC, 3rd, Daneshmand M, Kreienberg PB, Lee EC, Mehta M, et al. Outcome of aggressive surveillance colonoscopy in ruptured abdominal aortic aneurysm. J Vasc Surg 2004;39:792–6.
14. Zelenock GB, Strodel WE, Knol JA, Messina LM, Wakefield TW, Lindenauer SM, et al. A prospective study of clinically and endoscopically documented colonic ischemia in 100 patients undergoing aortic reconstructive surgery with aggressive colonic and direct pelvic revascularization, compared with historic controls. Surgery 1989;106:771–9; discussion 9–80.
15. Piotrowski JJ, Ripepi AJ, Yuhas JP, Alexander JJ, Brandt CP. Colonic ischemia: the Achilles heel of ruptured aortic aneurysm repair. Am Surg 1996;62:557–60; discussion 60–1.
16. Iwai T, Sakurazawa K, Sato S, Muraoka Y, Inoue Y, Endo M. Intraoperative monitoring of the pelvic circulation using a transanal Doppler probe. Euro J Vasc Surg 1991;5:71–4.
17. Conte MS. Bypass versus Angioplasty in Severe Ischaemia of the Leg (BASIL) and the (hoped for) dawn of evidence-based treatment for advanced limb ischemia. J Vasc Surg;51:69S–75S.
18. Takahashi M, Ishikawa T, Higashidani K, Katoh H. SPY: an innovative intra-operative imaging system to evaluate graft patency during off-pump coronary artery bypass grafting. Interact Cardiovasc Thorac Surg 2004;3:479–83.
19. Reuthebuch O, Haussler A, Genoni M, Tavakoli R, Odavic D, Kadner A, et al. Novadaq SPY: intraoperative quality assessment in off-pump coronary artery bypass grafting. Chest 2004;125:418–24.
20. Taggart DP, Choudhary B, Anastasiadis K, Abu-Omar Y, Balacumaraswami L, Pigott DW. Preliminary experience with a novel intraoperative fluorescence imaging technique to evaluate the patency of bypass grafts in total arterial revascularization. Ann Thorac Surg 2003;75:870–3.
21. Rubens FD, Ruel M, Fremes SE. A new and simplified method for coronary and graft imaging during CABG. Heart Surg Forum 2002;5:141–4.
22. Handa T, Katare RG, Sasaguri S, Sato T. Preliminary experience for the evaluation of the intraoperative graft patency with real color charge-coupled device camera system: an advanced device for simultaneous capturing of color and near-infrared images during coronary artery bypass graft. Interact Cardiovasc Thorac Surg 2009;9:150–4.
23. Piccolino FC, Borgia L, Zinicola E. Indocyanine green angiography of circumscribed choroidal hemangiomas. Retina 1996;16:19–28.
24. Flower RW, Hochheimer BF. A clinical technique and apparatus for simultaneous angiography of the separate retinal and choroidal circulations. Invest Ophthalmol 1973;12:248–61.
25. Kitai T, Miwa M, Liu H, Beauvoit B, Chance B, Yamaoka Y. Application of near-infrared time-resolved spectroscopy to rat liver — a preliminary report for surgical application. Phys Med Biol 1999;44:2049–61.
26. Kitai T, Inomoto T, Miwa M, Shikayama T. Fluorescence navigation with indocyanine green for detecting sentinel lymph nodes in breast cancer. Breast Cancer 2005;12:211–5.
27. Ohdaira H, Nimura H, Takahashi N, Mitsumori N, Kashiwagi H, Narimiya N, et al. The possibility of performing a limited resection and a lymphadenectomy for proximal gastric carcinoma based on sentinel node navigation. Surg Today 2009;39:1026–31.
28. Watanabe M, Tsunoda A, Narita K, Kusano M, Miwa M. Colonic tattooing using fluorescence imaging with light-emitting diode-activated indocyanine green: a feasibility study. Surg Today 2009;39:214–8.
29. Balacumaraswami L, Taggart DP. Digital tools to facilitate intraoperative coronary artery bypass graft patency assessment. Semin Thorac Cardiovasc Surg 2004;16:266–71.
30. Singh SK, Desai ND, Chikazawa G, Tsuneyoshi H, Vincent J, Zagorski BM, et al. The Graft Imaging to Improve Patency (GRIIP) clinical trial results. J Thorac Cardiovasc Surg;139:294–301.
31. Handa T, Katare RG, Nishimori H, Wariishi S, Fukutomi T, Yamamoto M, et al. New device for intraoperative graft assessment: HyperEye charge-coupled device camera system. Gen Thorac Cardiovasc Surg 2010;58:68–77.
32. D'Ancona G, Bartolozzi F, Bogers AJ, Pilato M, Parrinello M, Kappetein AP. Intraoperative graft patency verification in coro-

nary artery surgery: modern diagnostic tools. J Cardiothorac Vasc Anesth 2009;23:232–8.
33. Louagie YA, Haxhe JP, Jamart J, Buche M, Schoevaerdts JC. Doppler flow measurement in coronary artery bypass grafts and early postoperative clinical outcome. Thorac Cardiovasc Surg 1994;42:175–81.
34. Jaber SF, Koenig SC, BhaskerRao B, VanHimbergen DJ, Cerrito PB, Ewert DJ, et al. Role of graft flow measurement technique in anastomotic quality assessment in minimally invasive CABG. Ann Thorac Surg 1998;66:1087–92.
35. Desai ND, Miwa S, Kodama D, Koyama T, Cohen G, Pelletier MP, et al. A randomized comparison of intraoperative indocyanine green angiography and transit-time flow measurement to detect technical errors in coronary bypass grafts. J Thorac Cardiovasc Surg 2006;132:585–94.
36. Schmitz C, Ashraf O, Schiller W, Preusse CJ, Esmailzadeh B, Likungu JA, et al. Transit time flow measurement in on-pump and off-pump coronary artery surgery. J Thorac Cardiovasc Surg 2003;126:645–50.
37. Unno N, Suzuki M, Yamamoto N, Inuzuka K, Sagara D, Nishiyama M, et al. Indocyanine green fluorescence angiography for intraoperative assessment of blood flow: a feasibility study. Eur J Vasc Endovasc Surg 2008;35:205–7.

Nephrol Dial Transplant (2011) 26: 4023–4031
doi: 10.1093/ndt/gfr176
Advance Access publication 14 April 2011

Conditional *VHL* gene deletion activates a local NO–VEGF axis in a balanced manner reinforcing resistance to endothelium-targeted glomerulonephropathy

Taku Morita[1], Yoshihiko Kakinuma[2], Atsushi Kurabayashi[3], Mikiya Fujieda[1], Takayuki Sato[2], Taro Shuin[4], Mutsuo Furihata[3] and Hiroshi Wakiguchi[1]

[1]Department of Pediatrics, Kochi Medical School, Nankoku, Japan, [2]Department of Cardiovascular Control, Kochi Medical School, Nankoku, Japan, [3]Department of Pathology, Kochi Medical School, Nankoku, Japan and [4]Department of Urology, Kochi Medical School, Nankoku, Japan

Correspondence and offprint requests to: Yoshihiko Kakinuma; E-mail: kakinuma@kochi-u.ac.jp

Abstract

Background/aims. We have reported that tubular epithelial cell injury caused by renal ischemia–reperfusion is attenuated in conditional *VHL* knockout *(VHL-KO)* mice and also that induction of hypoxia-inducible factor (HIF) suppresses angiotensin II-accelerated Habu snake venom (HV) glomerulonephropathy in rats. However, it remains unknown whether *VHL* knockdown protects glomerular endothelial cells from endothelium-targeted glomerulonephritis.

Methods and results. *VHL-KO* mice with HV glomerulonephropathy (HV GN) had fewer injured glomeruli, a lower mesangiolysis score and reduced blood urea nitrogen levels. Immunoreactivity of vascular endothelial growth factor (VEGF) in the glomerular capillaries was enhanced by *VHL* knockdown and was conserved even in *VHL-KO* mice with HV GN, despite HV-attenuating endothelial VEGF expression *in vitro*. *VHL-KO* mice showed enhanced nitric oxide (NO) production in glomerular endothelial cells and tubular cells, associated with activated VEGF expression in the kidney (i.e. an activated NO–VEGF axis). The levels of NO in glomeruli and tubules were conserved even in mice with HV GN. In contrast, suppressing NO production in glomerular endothelial cells by an NO synthase inhibitor,

N_{ω}-nitro-L-arginase, completely blunted the protection of *VHL-KO* from HV GN. The activated NO-VEGF axis in the kidney of *VHL-KO* mice was also associated with an elevation in Flk-1 phosphorylation and increased levels of IL-10 and IP-10.

Conclusion. Conditional *VHL* knockdown may enhance the NO–VEGF axis and protect glomerular endothelial cells from HV GN, thereby providing resistance to injury of tubular epithelial cells and glomerular endothelial cells.

Keywords: Habu snake venom glomerulonephropathy; nitric oxide; vascular endothelial growth factor

Introduction

Using a model of acute glomerulonephopathy induced by Habu snake venom (HV GN) (a glomerular endothelium-targeted model), we have demonstrated that angiotensin II accelerates the formation of HV GN and that the kidneys are protected from glomerular injury by upregulation of a hypoxia-inducible factor (HIF)/vascular endothelial cell growth factor (VEGF) signaling pathway induced by cobalt chloride. In contrast, elevated von Hippel–Lindau protein (pVHL) exacerbates glomerular injury [1, 2]. Furthermore, using the Cre-lox P system in conditional *VHL* knockout *(VHL-KO)* mice, we demonstrated that renal tubular injury induced by ischemia–reperfusion injury was attenuated by deletion of *VHL* gene [3].

It is already known that the HIF system, represented by HIF-1α and HIF-2α, has a major role in protecting cells against hypoxic insult and that the level of these proteins is regulated by pVHL [4]. In hypoxia, disturbed interaction of HIF and VHL elevates the level of HIF-1α and upregulates downstream gene expression, including VEGF.

To date, we have carried out detailed investigations in conditional *VHL-KO* mice on the protective mechanism against acute renal tubular injury mediated by HIF-1, VEGF and downstream genes [3]. However, it remains unclear whether HIF-1α protein induction protects glomeruli from endothelial cell-targeted injuries. In *VHL-KO* mice, factors which are specifically responsible for cell protection remain difficult to be differentiated, as many downstream genes are simultaneously and sequentially transactivated by HIF-1α.

VEGF is one candidate that has a protective effect on glomerular capillary endothelial cells. Recently, it has been proposed that uncoupling of the VEGF–eNOS axis may trigger renal damage by upregulating VEGF expression and decreasing nitric oxide (NO) production [5]. This hypothesis suggests that eNOS-derived NO usually acts as a negative modulator against the effects of VEGF (i.e. proliferation of endothelial cells). Therefore, a balanced VEGF–eNOS axis appears to be needed for cell protection. On the basis of this hypothesis, pathological cell proliferation may result when the axis becomes unbalanced.

In this study, we used *VHL-KO* mice treated with HV to investigate the role of *VHL* gene knockdown on glomerular endothelial cells, with particular emphasis on the VEGF–eNOS axis.

Materials and methods

Cell culture

Human umbilical vein endothelial cells (HUVECs) were cultured in EGM-2 culture medium (Cambrex, Walkersville, MD) complemented with the suggested reagents and then treated with Habu snake venom (HV, 100 μg/mL, Sigma-Aldrich, St. Louis, MO) for 8 h. After this treatment, each sample was processed for western blot analysis.

Generation of VHL-KO mice

Mice carrying the floxed *VHL* allele were generated by Ma *et al.* [6], using Cre/lox site-specific recombination technology. To generate *VHL-KO* mice with inactivation in multiple tissues in an inducible manner, we crossed $VHL^{f/f}$ mice with $VHL^{d/+}$ mice which carried the tamoxifen-inducible Cre recombinase transgene, driven by a human β-actin promoter ($VHL^{f/d}CreER^{TM}$). To obtain an adequate number of mice for experiments, each $VHL^{f/d}CreER^{TM}$ mouse with the genetic background of C57BL6/J was crossed further to generate both $VHL^{f/f}CreER^{TM}$ *(VHL-KO)* mice and $VHL^{f/d}CreER^{TM}$ mice. One week before the experiments, the mice were injected intraperitoneally (i.p.) with tamoxifen in corn oil (4 mg/mouse) to activate Cre recombinase. For these experiments, 12–16-week-old male $VHL^{f/f}CreER^{TM}$ *(VHL-KO)* mice ($n = 11$), $VHL^{f/+}CreER^{TM}$ (*control*) mice ($n = 11$), heterogeneously VHL gene-deleted mice (*hetero VHL-KO*, i.e. $VHL^{del/+}$, $n = 3$) and *wild-type* mice (*wild-type*, $n = 3$) were administered tamoxifen to evaluate VEGF expression. The mice were housed in a specific pathogen-free facility, with routine serum analysis confirming they were negative for common murine viral pathogens.

Western blot analysis

Protein extracts from whole murine kidneys were prepared using Tissue Protein Extraction Reagent (Pierce Biotechnology, Rockfold, IL). Western blot analysis was performed as described in our previous study [7]. The protein extracts were mixed with sample buffer and the concentration of each sample was quantified precisely so that a comparable amount of protein was applied to each lane. The samples were separated by electrophoresis on sodium dodecyl sulfate–polyacrylamide gel electrophoresis gels and then transferred to polyvinylidene difluoride membranes (Immnbilion-P; Millipore, Bedford, MA). A rabbit polyclonal antibody against VHL (BD Bioscience), diluted at 1:500, and a polyclonal antibody against VEGF (Santa Cruz Biotechnology, Inc., Santa Cruz, CA), diluted at 1:200, were used in conjunction with a horseradish peroxidase-conjugated secondary antibody. The other primary antibodies used were against IL-10 (Abcam Inc., Cambridge, MA) diluted at 1:500; IP-10 (Abcam) diluted at 1:200; eNOS (Cell Signaling Technology, Danvers, MA) diluted at 1:200; phospho eNOS (Ser1177) (Cell Signaling Technology) diluted at 1:300 and phospho Flk-1 (Santa Cruz Biotechnology) diluted at 1:500. Comparability of sample loading volumes was confirmed by expression of α-tubulin and Coomassie brilliant blue staining.

A mouse model for Habu snake venom glomerulonephropathy

One week after *VHL-KO* mice had undergone unilateral nephrectomy, they were administered an intravenous injection of venom toxin *Trimeresurus flavoviridis* (6.5 mg/kg body weight, Sigma-Aldrich Chemicals) to induce Habu snake venom glomerulonephropathy (HV GN). This procedure was carried out according to modified protocols [1, 8]. One day after administration of HV, the mice were sacrificed for sampling, with some mice being processed by perfusion fixation. All the animals were housed in cages at a constant room temperature and humidity under a controlled light–dark cycle. The animals were fed with a standard diet. All the animal experiments were performed in accordance with the Japan Animal Protection Laws.

Tissue preparation

After the weight of the kidneys was measured, they were sliced transversely into 1-mm thick segments. Tissue sampling for morphometric analysis was performed using the area-weighted sampling technique, as described previously [9]. Paraffin sections that were 1–5 μm in thickness (five blocks per animal) were prepared for further study.

Semiquantitative analysis of mesangiolytic glomerular damage

A hallmark of HV GN is focal mesangiolysis, which is characterized by dissolution or disappearance of the mesangial matrix due to necrosis and